



1 Eddy enhanced primary production accelerates bacterial growth in the  
2 Eastern Tropical North Atlantic

3 Quentin Devresse<sup>1</sup>, Kevin W. Becker<sup>1</sup>, Arne Bendinger<sup>1,2</sup>, Johannes Hahn<sup>1,3</sup>, Anja Engel<sup>1</sup>

4 <sup>1</sup>GEOMARHelmholtz Centre for Ocean Research Kiel, Germany,

5 <sup>2</sup>Laboratoire d'Etudes en Géophysique et Océanographie Spatiales (LEGOS), Université Toulouse,  
6 IRD, CNRS, CNES, UPS, Toulouse, France

7 <sup>3</sup>Bundesamt für Seeschifffahrt und Hydrographie, Hamburg, Germany

8

9 Correspondence: Quentin Devresse (qdevresse@geomar.de)

10

11 **Abstract**

12 Mesoscale eddies play essential roles in modulating the ocean's physical, chemical, and  
13 biological properties. In cyclonic eddies (CE) nutrient upwelling can stimulate primary  
14 production by phytoplankton. Yet, how this locally enhanced autotrophic production affects  
15 heterotrophic bacterial activities (biomass production and respiration) and consequently the  
16 metabolic balance between the synthesis and the consumption of dissolved organic matter  
17 (DOM) remains largely unknown. To address this gap, we investigated the horizontal and  
18 vertical variability of phytoplankton and heterotrophic bacterial activity along ~900 km zonal  
19 corridor between the coast of Mauretania and the Cape Verde Islands in the eastern tropical  
20 North Atlantic (ETNA). We additionally collected samples from a CE along this transect at  
21 high spatial resolution. Our results show cascading effects of physical disturbances induced by  
22 a CE on phyto- and bacterioplankton biomass and metabolic activities. Specifically, the  
23 injection of nutrients into the sunlit surface resulted in enhanced autotrophic plankton  
24 abundance and activity as indicated by Chlorophyll *a* (Chl-*a*) concentration, DOM exudation,  
25 and primary productivity (PP). However, the detailed eddy survey revealed an uneven  
26 distribution of these parameters with, for example, the highest Chl-*a* concentrations and PP  
27 rates near and just beyond the CE's periphery. The heterotrophic bacterial activity was similarly  
28 variable. Optode-based bacterial respiration (BR) and biomass production (BP) largely  
29 followed the trends of PP and Chl-*a*. Thus, a submesoscale spatial mosaic of heterotrophic  
30 bacterial abundance and activities occurred within the CE studied here that was closely related  
31 to variability in autotrophic production. This was supported by a significant positive correlation



32 between concentrations of semi-labile organic carbon (SL-DOC; the sum of dissolved  
33 hydrolyzable amino acids and combined carbohydrates) and BR measurements. Bacterial  
34 growth efficiency ( $BP/(BR+BP)$ ) was variable (1.4-10.5%) within the CE and carbon  
35 exudation was not always sufficient to compensate the bacterial carbon demand ( $BR+BP$ ; 28.3-  
36 114.5%). We have additionally estimated the metabolic state in our samples, which showed that  
37 the CE carried a strong autotrophic signal ( $PP/(BR+BP)>1$ ). Overall, our results show that  
38 submesoscale (0-10 km) processes lead to highly variable metabolic activities of both  
39 phototrophic and heterotrophic microbes, which has implications for biogeochemical models  
40 estimating oceanic carbon fluxes. Additionally, we revealed that the CE not only traps and  
41 transports coastal nutrients and carbon to the open ocean but also stimulates phytoplankton  
42 growth generating freshly produced organic matter during westward propagation. This organic  
43 matter may fuel heterotrophic processes in the open ocean and may help to explain the often-  
44 observed net heterotrophic metabolic state of these environments.

45

## 46 1. Introduction

47

48 Mesoscale eddies (10-100 km) are ubiquitous in the ocean affecting upper ocean  
49 biogeochemistry and ecology, e.g. upwelling nutrients influencing primary production and  
50 carbon export (Cheney and Richardson, 1976; Aristegui et al., 1997). The sense of rotation and  
51 their vertical structure classifies cyclonic (CEs), anticyclonic (ACEs; e.g. Chelton et al., 2011)  
52 or anticyclonic mode water eddies (ACMEs; D'Asaro 1988). In Eastern Boundary Upwelling  
53 Systems (EBUS), eddies may form by flow separation of along slope boundary currents at  
54 topographic headlands (D'Asaro 1988, Molemaker et al., 2015, Thomsen et al., 2016). Eddies  
55 have lifespans from days to months and can travel several hundred to thousands of kilometers  
56 across ocean basins (Chelton et al., 2011). They are complex dynamical regimes for organic  
57 matter and nutrient transport (Gruber et al., 2011). In the North Atlantic Ocean, eddies  
58 generated in the highly productive Canary Upwelling System (CanUS) may laterally propagate  
59 to the oligotrophic Subtropical North Atlantic Gyre (SNAG), transporting thereby nutrients and  
60 carbon (McGillicuddy et al., 2003; Karstensen et al., 2015; Schütte et al., 2016). A variety of  
61 studies demonstrated the impact of eddies on primary production (PP) on a global scale. Yet,  
62 the magnitude of the eddy-induced flux and its utilization depend on the model, the area  
63 investigated, and the degree of resolution and is still controversial (See review by  
64 McGillicuddy, 2016 and references therein). For example, Couespel et al., (2021) performed



65 global warming simulations using a representation of mid-latitude double-gyre circulation and  
66 showed that at the finest model resolution ( $1/27^\circ$ ), eddies can mitigate the decline of primary  
67 production ( $-12\%$  at  $1/27^\circ$  vs.  $-26\%$  at  $1^\circ$ ). Modeling studies have long urged consideration  
68 of the effects of eddies on PP at submesoscale levels (0.1-10 km) to provide realistic estimates  
69 of the oceanic carbon cycle (Levy et al., 2001). Thus, understanding the impact of mesoscale  
70 eddies on plankton productivity will help to better predict future carbon cycling in EBUS under  
71 global change scenarios.

72 Eddies modulate the mixed layer depth by upwelling (CEs), downwelling (ACEs), or  
73 frontogenesis from eddy-eddy interaction, thereby creating spatial variability of nutrient  
74 concentration within/around eddies on length scales of 0.1-10 km (see reviews by Mahadevan,  
75 2016 and McGillicuddy, 2016). In addition, the nonlinear response of phytoplankton growth to  
76 nutrient availability and advection of phytoplankton by currents makes plankton distribution  
77 and community composition highly variable within and around eddies (Lochte and Pfannkuche  
78 1987). As a consequence, the spatial distribution of PP across eddies can be highly variable  
79 (e.g. Falkowski et al., 1991; Ewart et al., 2008; Singh et al., 2015). Still, insight into the  
80 distribution of phytoplankton and their activities within mesoscale eddies is limited due to a  
81 lack of sufficient fine-scale vertical and horizontal resolution studies to adequately describe  
82 these distributions.

83 Bacterial activity is directly coupled to PP: autotrophic cells release dissolved organic matter  
84 (DOM), the main substrate for heterotrophic bacteria and archaea (Thornton 2014). DOM  
85 release has been interpreted as a cellular overflow mechanism that expels the carbon produced  
86 in excess (Wood and Van Valen, 1990; Schartau et al., 2007). Therefore, released DOM  
87 compounds are often depleted in nutrients limiting autotrophic cell growth (Engel et al., 2002).  
88 Patchiness of phytoplankton primary productivity and nutrient limitation within eddies may  
89 thus lead to spatial heterogeneity of extracellular release rates (e.g. Lasternas et al., 2013, Rao  
90 et al., 2021) with distinct quality (e.g. Wear et al., 2020). DOM quality impacts biomass  
91 production (BP), bacterial respiration (BR), and, thus the bacterial growth efficiency (BGE;  
92 Neijssel and de Mattos, 1994; Russell and Cook, 1995). BGE is the ratio between BP and the  
93 bacterial carbon demand (BCD), which is the sum of assimilated carbon that is respired and  
94 carbon that is incorporated into biomass (BP + BR). Lønborg et al., (2011) established that BGE  
95 decreases with increasing C/N ratio of the bioavailable DOM produced by phytoplankton. BGE  
96 is a critical parameter for estimating the amount of consumed organic carbon that is used to  
97 build biomass by heterotrophic bacteria (Anderson and Ducklow 2001). So far, BGE within



98 eddies has been reported for ACEs from the Mediterranean Sea (Christaki et al., 2011), but not  
99 for CE and Mode Water Eddies. In general, several studies showed a patchy distribution of  
100 bacterial abundance, BP (Ewart et al., 2008; Baltar et al., 2010), BR, community respiration  
101 (CR) (Mouriño-Carballido and McGillicuddy 2006; Mouriño-Carballido, 2009), and of the  
102 metabolic balance between production and consumption of organic matter (Maixandeu et al.,  
103 2005; Ewart et al., 2008; Mouriño-Carballido and McGillicuddy 2006; Mouriño-Carballido,  
104 2009) within eddies.

105 Yet, how eddies affect microbial plankton dynamics and carbon flow is largely unknown. So  
106 far, phyto- and bacterioplankton distribution and activities were either studied separately or at  
107 relatively low spatial resolution. Data on eddy-induced changes in primary production,  
108 extracellular release and semi-labile DOM concentration, and the responses of heterotrophic  
109 microbial metabolic activities are scarce. Understanding how eddies modulate microbial  
110 activities will enhance our knowledge about the fate of autotrophically fixed organic carbon  
111 and the overall CO<sub>2</sub> source/sink function in the ocean, and in particular EBUS.

112 Here, we studied the impact of a CE on microbial carbon cycling along a zonal corridor of the  
113 westward propagating eddies between the Cape Verde Islands and the Mauretania Upwelling  
114 System (13-20 °N), a sub-region of the CanUS (13-33 °N, Aristegui et al., 2009). About  $146 \pm 44$   
115 eddies with a lifetime of more than 7 days are generated per year in this region (Schütte et al.,  
116 2016). Along this corridor, we determined phytoplankton (<20µm) cell abundance, primary  
117 production, and extracellular release. We linked those parameters of autotrophic activity to  
118 semi-labile DOM concentration and heterotrophic bacterial activity. Our study gives new  
119 insights into 1) microbial carbon cycling and 2) factors controlling microbial metabolic  
120 activities within and around CE formed in EBUS.

121

## 122 2. Materials and Methods

123

### 124 2.1 Study area and eddy characterization

125

126 Sampling was conducted in the ETNA between the Cape Verde archipelago and the  
127 Mauritanian coast during cruise M156 (July 3<sup>rd</sup> to August 1<sup>st</sup>, 2019. Figure 1A) on the R/V  
128 *Meteor*. Samples were collected during the relaxation period (from May to July) that follows  
129 the upwelling season (January to March; Lathuilière et al., 2008). A CE was sampled at high



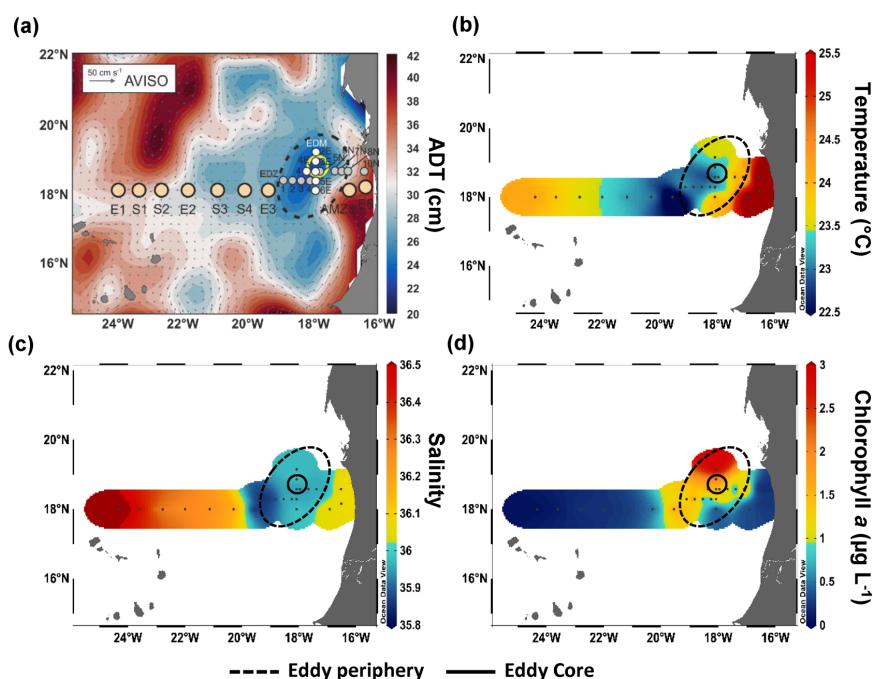
130 spatial resolution along two zonal (from 19.1 °W to 18.2 °W at 18.3 °N and from 18.5 °W to  
131 17.1 °W at 18.6 °N) and one meridional transects (from 19.4 °N to 18 °N at 18.4 °W to 18.1  
132 °W). The zonal section was slightly meridionally shifted east/west of the eddy core position.  
133 The reason for that was the deformed eddy shape, which resulted in a consecutive optimized  
134 identification of the eddy core position during the eddy survey. In addition, we sampled water  
135 along the 18 °N transect, a typical coast to open ocean trajectory of eddies in the region (Schütte  
136 et al., 2016). Salinity, temperature, depth, and O<sub>2</sub> concentration were determined at each station  
137 using a Seabird 911 plus CTD system equipped with two independently working sets of  
138 temperature-conductivity-oxygen sensors. The oxygen sensor was calibrated against discrete  
139 water samples using the Winkler method (Strickland and Parsons, 1968; Wilhelm, 1888).  
140 Seawater samples were collected from the top 200 m using 10L Niskin bottles attached to the  
141 CTD Rosette. A total of 25 stations were sampled; 14 of them inside or in the vicinity of the  
142 CE. Sampling was conducted in the epipelagic layer (0-200 m), including water from the  
143 surface, within the mixed layer, at the Chl-*a* maximum, and within the shallow oxygen  
144 minimum zone (OMZ; <50 μmol kg<sup>-1</sup> between 0-200 m depth) when present.

145 Sea surface height (SSH) and Acoustic Doppler Current Profiler (ADCP) velocity data (SI Fig.  
146 **1**), characterized the eddy as a CE. Based on the Angular Momentum Eddy Detection and  
147 Tracking Algorithm (AMEDA; Le Vu et al., 2018), the eddy was estimated to be 1.5 months  
148 old. The center of the eddy and the core radius were determined using ADCP reconstruction  
149 assuming an axis-symmetric vortex. (SI Fig. **1**). On 22/07/2019, the eddy center was located at  
150 18.69 °N, 18.05 °W, with a core radius of 40.5 ± 5.7 km. The mean azimuthal velocity in the  
151 CE was 19.9 ± 0.7 cm s<sup>-1</sup> and the absolute dynamic topography associated with the CE core  
152 was ~23 cm on 23/07/19. Fine-scale analysis of the eddy physics will be given by Fischer et al.  
153 (2022, in prep). However, as the eddy shape was deformed, ADCP reconstruction did not  
154 constrain well the physical border of the eddy (SI Fig. **1**). Therefore, we combined sea surface  
155 temperature (23.44 ± 0.47 °C) salinity (39.95 ± 0.04) and Chl-*a* (1.35 ± 0.73 μg L<sup>-1</sup>) data to  
156 approximate the area influenced by the eddy (Fig. **1b,c,d**). We classified stations into ‘core’  
157 and ‘periphery’ of the eddy. Stations that were outside and westward of the eddy influence were  
158 referred to as ‘open ocean’ and those close to the coast as ‘coastal’. At the St. E3, outside of the  
159 CE periphery, we observed a front with surface temperature and salinity (not compensating in  
160 density) being clearly different from among the adjacent stations (Fig. **1b**), potentially which  
161 might be related to enhanced, an up- and downwelling might have occurred there on either side  
162 of the front, respectively. Hence, we referred to that station as ‘Frontal Zone’. The classification



163 of stations is thoroughly discussed in the supplementary information (SI), and the sampling  
164 time, location, and distance from the eddy center are given in Table S1.

165



166

167 Figure 1: M156 cruise track (a) Temperature at 5m depth (b) Salinity at 5m depth (c) chlorophyll a at  
168 5m depth (d). The color background in (a) shows the variations in Absolute Dynamic Topography  
169 (ADT). The direction and speed of surface water geostrophic currents are shown as arrows.

170

## 171 2.2 Chemical analyses

172 Nutrient concentrations were determined at selected stations (SI Table 1). Nutrients were  
173 measured onboard from duplicate samples (11 mL) of unfiltered seawater samples. Ammonium  
174 ( $\text{NH}_4^+$ ) was analyzed after Solórzano (1969) and phosphate ( $\text{PO}_4$ ), nitrate ( $\text{NO}_3$ ), nitrite ( $\text{NO}_2$ ),  
175 and silicate ( $\text{Si}(\text{OH})_4$ ) were measured photometrically with continuous-flow analysis on an  
176 auto-analyzer (QuAatro; Seal Analytical) after Grasshoff et al., (1999). Detection limits for  
177  $\text{NH}_4^+$ ,  $\text{PO}_4$ ,  $\text{NO}_3$ ,  $\text{NO}_2$ , and  $\text{Si}(\text{OH})_4$  were 0.1, 0.02, 0.1, 0.02, and 0.2  $\mu\text{mol L}^{-1}$ , respectively  
178 Total dissolved inorganic nitrogen (DIN) was determined as the sum of  $\text{NH}_4^+$ ,  $\text{NO}_3$ , and  $\text{NO}_2$ .



179 To estimate the fraction of semi-labile dissolved organic carbon (DOC), we determined high-  
180 molecular-weight (HMW > 1 kDa) dissolved combined carbohydrates (dCCHO) and dissolved  
181 amino acids (dAA) as the main biochemical components of DOM.

182 Duplicate samples (20 mL) for dCCHO were filtered through 0.45 µm Acrodisk filters,  
183 collected in combusted glass vials (8 h, 450 °C) and frozen (−20 °C) until analysis after Engel  
184 & Händel (2011) with a detection limit of 1 µg L<sup>−1</sup>. The analysis detected 11 monomers:  
185 arabinose, fucose, galactose, galactosamine, galacturonic acid, glucosamine, glucose,  
186 glucuronic acid, rhamnose, co-elute mannose, and xylose.

187 Duplicate samples (4 mL) for dHAA were filtered through 0.45µm Acrodisk filters, collected  
188 in combusted glass vials (8 h, 450 °C), and frozen (−20 °C) until analysis. dAA were measured  
189 with ortho- phthaldialdehyde derivatization by high-performance liquid chromatography  
190 (HPLC; Agilent Technologies, USA) equipped with a C<sub>18</sub> column (Phenomenex, USA)  
191 (Lindroth and Mopper, 1979; Dittmar et al., 2009). The analysis classified 13 monomers with  
192 a precision < 5 % and a detection limit of 2 nmol L<sup>−1</sup>: alanine, arginine, aspartic acid, isoleucine,  
193 glutamic acid, glycine, leucine, phenylalanine, serine, threonine, tyrosine, valine; and γ-  
194 aminobutyric acid (GABA).

195 The calculations for the carbon content of dCCHO and dHAA were based on carbon atoms  
196 contained in the identified monomers. The sum of dCCHO and dHAA carbon content is referred  
197 to as semi-labile DOC (SL-DOC).

198 For Chl-*a*, 1L samples were collected on 25 mm GF/F (Whatman, GE Healthcare Life Sciences,  
199 UK) and subsequently frozen (−20 °C) until extraction using 90 % acetone for photometric  
200 analyses (Turner Designs, USA), slightly modified after Evans et al., (1987).

201 Bacteria were quantified using a flow cytometer (FACSCalibur, Becton Dickinson, Oxford,  
202 UK). Seawater samples (1.7 mL) were fixed with 85 µL glutaraldehyde (1% final  
203 concentration) and stored at -80 °C until enumeration. Samples were stained with SYBR Green  
204 I (molecular probes) and were enumerated with a laser emitting at 488 nm and detected by their  
205 signature in a plot of side scatter (SSC) vs green fluorescence (FL1). Heterotrophic bacteria  
206 were distinguished from photosynthetic bacteria (*Prochlorococcus* and *Synechococcus*) by their  
207 signature in a plot of red fluorescence (FL2) vs green fluorescence (FL1). Yellow-green latex  
208 beads (1 µm, Polysciences) were used as an internal standard. (Stolle et al., 2009). Cell counts  
209 were determined with the CellQuest software (Becton Dickinson). For autotrophic pico and  
210 nanoplankton <20 µm, 2 mL samples were fixed with formaldehyde (1 % final concentration)





211 and stored frozen ( $-80^{\circ}\text{C}$ ) until analysis. Red and orange autofluorescence was used to identify  
212 Chl-*a* and phycoerythrin cells. Cell counts were determined with CellQuest software (Becton  
213 Dickinson); picoplankton and nanoplankton populations containing Chl-*a* and/or phycoerythrin  
214 (i.e., *Synechococcus*) were identified and enumerated. We converted the cell abundance of the  
215 different autotrophic plankton populations into biomass assuming  $43\text{ fg C cell}^{-1}$  for  
216 *Prochlorococcus*,  $120\text{ fg C cell}^{-1}$  for *Synechococcus*,  $500\text{ fg C cell}^{-1}$  for eukaryotic picoplankton  
217 and,  $3.100\text{ fg C cell}^{-1}$  for eukaryotic nanoplankton after Hernández-Hernández et al., (2020).  
218 We report the autotrophic plankton biomass as the sum of eukaryotic pico- and nanoplankton  
219 and cyanobacteria (*Prochlorococcus* and *Synechococcus*) biomass. The abundance of  
220 eukaryotic pico- and nanoplankton and cyanobacteria (*Prochlorococcus* and *Synechococcus*)  
221 can be found in the SI (Table S2).

222

### 223 2.3 Microbial activities

224 More information on procedures and calculations of microbial activities are given in the SI.

225 Bacterial biomass production rates (BP) were measured through the incorporation of labeled  
226 leucine ( $^3\text{H}$ ) (specific activity  $100\text{ Ci mmol}^{-1}$ , Biotrend) using the microcentrifuge method  
227 (Kirchman et al., 1985; Smith and Azam, 1992). Duplicate samples and one killed control ( $1.5$   
228 mL each) were labeled using  $^3\text{H}$ -leucine at a final concentration of  $20\text{ nmol L}^{-1}$  and incubated  
229 with headspace for 6 h in the dark at  $14^{\circ}\text{C}$ . Controls were poisoned with trichloroacetic acid.  
230 All Samples were measured on board with a liquid scintillation analyzer (Packard Tri-Carb,  
231 model 1900 A).  $^3\text{H}$ -leucine uptake was converted to carbon units applying a conversion factor  
232 of  $1.55\text{ kg C mol}^{-1}$  leucine (Simon and Azam, 1989).

233 BP rates at  $22^{\circ}\text{C}$  were estimated following López-Urrutia and Morán (2007):

$$234 \quad \text{BP}_{22^{\circ}\text{C}} = \text{BP}_{14^{\circ}\text{C}} \times 0.996 \quad (\text{Eq. 1})$$

235 Community respiration rates (CR) were estimated from changes of dissolved oxygen in 24-36  
236 hours incubations at  $14^{\circ}\text{C}$  using optode spot mini sensors (PreSens PST3; Precision Sensing  
237 GmbH, Regensburg, Germany). The detection limit (DL) for CR was  $0.55\text{ }\mu\text{mol O}_2\text{ L}^{-1}\text{ d}^{-1}$ .

238 CR at  $22^{\circ}\text{C}$  was estimated using extrapolation from Regaudie-De-Gioux and Duarte (2012):

$$239 \quad \text{CR}_{22^{\circ}\text{C}} = \text{CR}_{14^{\circ}\text{C}} \times 2.011 - 0.013 \quad (\text{Eq. 2})$$

240  $\text{CR}_{22^{\circ}\text{C}}$  was converted into bacterial respiration ( $\text{BR}_{22^{\circ}\text{C}}$ ) after Aranguren-Gassis et al. (2012):





241 
$$BR_{22^{\circ}\text{C}} = 0.30 \times CR_{22^{\circ}\text{C}}^{1.22} - 0.013 \quad (\text{Eq. 3})$$

242 A respiratory quotient of 1 was used to convert oxygen consumption into carbon respiration  
243 (del Giorgio and Cole 1998).

244 We furthermore estimated the bacterial carbon demand (BCD):

245 
$$BCD = BP + BR \quad (\text{Eq. 4})$$

246 and the bacterial growth efficiency (BGE):

247 
$$BGE = \frac{BP}{BCD} \quad (\text{Eq. 5})$$

248 Primary production (PP) was determined from  $^{14}\text{C}$  incorporation according to Steemann  
249 Nielsen (1952) and Gargas (1975). Polycarbonate bottles (Nunc EasYFlask, 75 cm<sup>2</sup>) were filled  
250 with 260 mL prefiltered (mesh size of 200 μm) sample and spiked with 50 μL of a ~11 μCi  
251  $\text{NaH}^{14}\text{CO}_3^-$  solution (Perkin Elmer, Norway). 200 μL were removed immediately after spiking  
252 and transferred to a 5 mL scintillation vial for determination of added activity. Then, 50 μL of  
253 2N NaOH and 4 mL scintillation cocktail (Ultima Gold AB) were added. Duplicate samples  
254 were incubated in 12 h light and 12 h dark at 22 °C. Three light levels were applied: 1200-1400;  
255 350 and 5 μE, with high values representing surface irradiance at the time of sampling. The  
256 incubation length was chosen for two reasons. First, we expected low productivity of the open  
257 ocean phytoplankton community due to low biomass and low nutrient concentrations at the start  
258 of the incubation. Under these conditions, short-term incubations of only a few hours may  
259 underestimate PP, because carbon assimilation by algal cells may be too low to discriminate  
260 against  $^{14}\text{C}$  adsorption as determined in blank dark incubation (Engel et al., 2013). Moreover,  
261 the release of freshly assimilated carbon into the DOM pool has a time scale of several hours  
262 because of the equilibration of the tracer and because metabolic processes of organic carbon  
263 exudation follow those of carbon fixation inside the cell (Engel et al., 2013). Incubations were  
264 stopped by filtration of a 70 mL sub-sample onto 0.4 μm polycarbonate filters (Nuclepore).  
265 Particulate primary production (PP<sub>POC</sub>) was determined from material collected on the filter,  
266 while the filtrate was used to determine dissolved primary production (PP<sub>DOC</sub>). All filters were  
267 rinsed with 10 mL sterile filtered (<0.2 μm) seawater, and then acidified with 250 μL 2N HCl  
268 to remove inorganic carbon (Descy et al., 2002). Filters were transferred into 5 mL scintillation  
269 vials, and 4 mL scintillation cocktail (Ultima Gold AB) was added. To determine PP<sub>POC</sub> and  
270 PP<sub>DOC</sub>, 4 mL of filtrate and incubated sample were transferred to 20 mL scintillation vials,  
271 acidified (100 μL 1N HCl), and left open in the fume hood to remove inorganic carbon. Then,



272 100  $\mu\text{L}$  of 2N NaOH and 15 mL scintillation cocktail were added. All samples were counted  
273 the following day in a liquid scintillation analyzer (Packard Tri-Carb, model 1900 A).

274 Primary production (PP) of organic carbon was calculated according to Gargas (1975):

275

$$276 \quad \text{PP } (\mu\text{molC L}^{-1} \text{ d}^{-1}) = \frac{a2 \times \text{DI}^{12\text{C}} \times 1.05 \times k_1 \times k_2}{a1} \quad (\text{Eq.6})$$

277

278 Where  $a1$  and  $a2$  are the activities (DPM) (disintegrations per minute) of the added solution  
279 and the sample corrected for dark sample, respectively, and  $\text{DI}^{12\text{C}}$  is the concentration ( $\mu\text{mol}$   
280  $\text{L}^{-1}$ ) of dissolved inorganic carbon (DIC) in the sample. Dissolved inorganic carbon  
281 concentration was calculated from total alkalinity using r package seacarb (Gattuso et al., 2020).  
282 Total alkalinity of the seawater was acquired through the open-cell titration method (Dickson  
283 et al., 2007). The value 1.05 is a correction factor for the discrimination between  $^{12}\text{C}$  and  $^{14}\text{C}$ ,  
284 as the uptake of the  $^{14}\text{C}$  isotope is 5% slower than the uptake of  $^{12}\text{C}$ ,  $k_1$  is a correction factor  
285 for subsampling (bottle volume/filtered volume) and  $k_2$  is the incubation time ( $\text{d}^{-1}$ ). Total  
286 primary production ( $\text{PP}_{\text{TOT}}$ ;  $\mu\text{mol C L}^{-1} \text{ d}^{-1}$ ) was derived from the sum of  $\text{PP}_{\text{POC}}$  and  $\text{PP}_{\text{DOC}}$   
287 according to:

288

$$289 \quad \text{PP}_{\text{TOT}} = \text{PP}_{\text{POC}} + \text{PP}_{\text{DOC}} \quad (\text{Eq.7})$$

290

291 The percentage of extracellular release (PER; %) was calculated as:

$$292 \quad \text{PER} = \left( \frac{\text{PP}_{\text{DOC}}}{\text{PP}_{\text{TOT}}} \right) \times 100 \quad (\text{Eq.8})$$

293

## 294 2.4 Data analysis

295 Statistical analyses and calculations were conducted using the software R (v4.0.3) in Rstudio  
296 (v1.1.414; Ihaka and Gentleman 1996). Analysis of variances (ANOVA) and Tukey test, were  
297 performed on the different parameters by grouping the station by their position (SI Table 1).  
298 Seawater density was calculated using r package oce v1.3.0 (Kelley, 2018) and mixed layer  
299 maximum depth was determined as the depth at which a change from the surface density of  
300 0.125 has occurred (Levitus, 1982). Section plots were realized using Ocean Data View  
301 (Schlitzer, 2020). Other packages used in this study include corrplot v0.84 (Dray, 2008) and  
302 ggplot2 v3.3.3 (Wickham, 2016). Depth integrated values were calculated using the midpoint  
303 rule.



### 304 3. Results

305

#### 306 3.1 Hydrographic conditions

307 Along the zonal transect, open ocean waters (from 20 to 24.5 °W) had a temperature range of  
308 17.0-24.3 °C and salinity of 36.19-36.79 in the upper 150m depth (Fig. **2a & b**). The average  
309 mixed layer depth was  $30 \pm 2$  m (SI Table 1). Oxygen concentration (Fig. **2c**) decreased with  
310 depth while nutrient concentrations increased (Fig. **2d-e**). Nutrients were depleted ( $<0.5$ ,  $<0.2$ ,  
311 and  $<0.5 \mu\text{mol L}^{-1}$  for DIN, PO<sub>4</sub>, Si(OH)<sub>4</sub>, respectively) in the mixed layer.

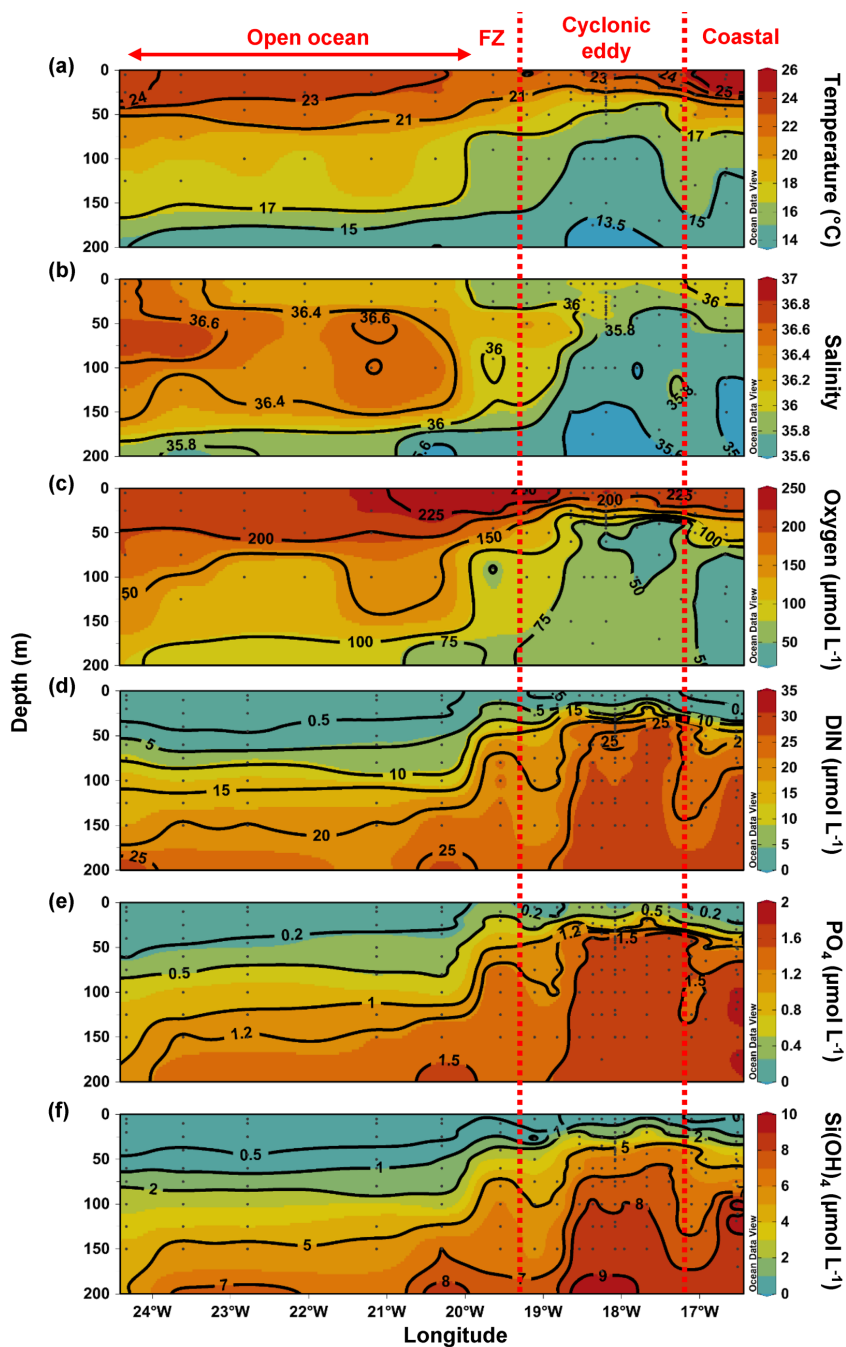
312 At the coastal stations (16.51 to 16.92 °W), the temperature had a range of 14.6-26.1 °C and  
313 salinity of 35.53-36.08 in the upper 150 m depth (Fig. **2a & b**). Here, the mixed layer was  
314 significantly shallower than in the open ocean (Tukey,  $p<0.01$ ), with an average depth of  $17 \pm$   
315  $4$  m (SI Table 1). Oxygen was decreasing with depth and a shallow oxygen minimum (OMZ;  
316  $<50 \mu\text{mol kg}^{-1}$ ) was detected (Fig. **2c**) from 80 m to 200 m depth. Nutrients (Fig. **2d-e**) were  
317 depleted at the surface (5 m depth) while the deeper coastal waters (~ 80 to 200 m depth) were  
318 colder and richer in nutrients than in the open ocean with on average 3.4 fold more nutrients  
319 (DIN, PO<sub>4</sub>, Si(OH)<sub>4</sub>) when integrated over 100 m depth.

320 In the CE ('periphery' and 'core'), waters had a temperature (range of 13.5-24.2 °C and salinity  
321 of 35.48-36.36 in the upper 150 m depth (Fig. **2a & b**). A tightening of isopycnals with a strong  
322 doming of the isotherms, isohalines, and nutriclines was observed (Fig. **2a-b, d-f**). A shallow  
323 OMZ was detected from ~30m to ~100 m depth with the lowest oxygen concentration ( $<10$   
324  $\mu\text{mol kg}^{-1}$ ) between 30-40 m depth. The mixed layer was significantly shallower (Tukey,  
325  $p<0.05$ ) at the CE periphery than in the open ocean, with an average of  $15 \pm 6$  m depth.  
326 However, the CE core was not significantly different ( $21 \pm 3$  m; Tukey,  $p>0.05$ ). Nutrients (Fig.  
327 **2d-f**) were depleted ( $<0.5$ ,  $<0.2$  and  $<0.5 \mu\text{mol L}^{-1}$  for DIN, PO<sub>4</sub>, Si(OH)<sub>4</sub> respectively) at the  
328 surface (~5 m) only in the Eastern (17.11 °W, 18 °N) and Western (18.83-19.11 °W, 18.58 °N)  
329 part of the CE periphery.

330 The Frontal Zone station E3 (19.55 °W) was distinct from the adjacent stations with respect to  
331 surface temperature (1 °C colder, Fig **2a**). A doming of the nutriclines was observed (Fig.**2d-f**)  
332 and nutrient concentrations integrated over 100 m depth at St. E3 were ~3 fold higher than Open  
333 ocean St. S4 (20.3 °W) and ~1.2 fold higher than CE periphery St. EDZ-1 (19.11 °W).

334

335



336

337 Figure 2: Epipelagic distribution (0-200m) of Temperature (a), Salinity (b), Oxygen (c), Total inorganic  
338 nitrogen (DIN, d),  $\text{PO}_4$  (e),  $\text{Si(OH)}_4$  (f). Red dashed line show the cyclonic eddy periphery and FZ refer  
339 as Frontal Zone.



### 340 3.2 Chlorophyll-*a* and primary production

341 In order to compare stations along the zonal transect and within the eddy, data were integrated  
342 over the water column (0-100 m depth). Along the zonal transect, depth-integrated Chl-*a*  
343 concentration ranged between 11.7 and 58.7 mg m<sup>-2</sup> and decreased from the coastal to the open  
344 ocean stations (Table 1; SI Fig. S4). Depth-distribution (Fig. 3a) presented a Chl-*a* maximum  
345 in the open ocean around ~75 m from 23.61 to 24.33 °W and around ~50 m from 22.78 to 20.3  
346 °W, up to 0.70 µg L<sup>-1</sup>. At the coastal stations, the Chl-*a* maximum was found between 30-40 m  
347 depth with values up to 0.96 µg L<sup>-1</sup>. Integrated autotrophic plankton biomass (Table 1) ranged  
348 between 1.6 and 7.8 and between 3.6 and 6.1 g C m<sup>-2</sup> in the open ocean and at the coastal  
349 stations, respectively. In the open ocean waters, autotrophic plankton biomass (Fig. 3b)  
350 presented a gradient of distribution with a maximum around ~75 m from 23.61 to 24.33 °W,  
351 around ~50 m from 22 to 22.78 °W and between 5-25 m from 21.13 to 20.3 °W, with values up  
352 to 166 µg C L<sup>-1</sup>. In the coastal stations, autotrophic plankton biomass maximum was found  
353 between 30-40 m depth with values up to 117 µg C L<sup>-1</sup>. Both Chl-*a* concentration and  
354 autotrophic plankton biomass did not vary significantly between the open ocean and the coastal  
355 stations (Tukey,  $p > 0.05$ ). Integrated total and dissolved primary production (PP<sub>TOT</sub>; PP<sub>DOC</sub>;  
356 Table 1) remained fairly constant with ranges of 101-137 and 42.8-78 mmol C m<sup>-2</sup> d<sup>-1</sup>,  
357 respectively, from the coastal to the open ocean stations, except for the station furthest offshore  
358 (24.33 °W), where rates decreased sharply to 25.8 mmol C m<sup>-2</sup> d<sup>-1</sup> for PP<sub>TOT</sub> and to 12.3 mmol  
359 C m<sup>-2</sup> d<sup>-1</sup> for PP<sub>DOC</sub>. The integrated percentage of extracellular release (PER; Table 1) in both  
360 regions ranged between 42.3-67.5%. Both PP<sub>TOT</sub> and PER did not vary significantly between  
361 the open ocean and the coastal stations (Tukey,  $p > 0.05$ ). PP<sub>TOT</sub> was decreasing with depth (Fig.  
362 3c) while PER was increasing (Fig. 3d). In general, PP<sub>TOT</sub> and PP<sub>DOC</sub> were positively correlated  
363 to the Chl-*a* concentration ( $R^2 = 0.48$  and  $0.42$  respectively;  $p < 0.001$ ; Fig. 6c & d).

364 In the CE (core and periphery) and at the Frontal Zone integrated Chl-*a* concentration ranged  
365 from 17.2 to 225 mg m<sup>-2</sup> (Table 1). The Chl-*a* distribution (SI Fig. S4) showed a clear spatial  
366 separation with the highest values (98.7-225 mg m<sup>-2</sup>) in the western (18.83-19.11 °W, 18.29  
367 °N) and northern (148 mg m<sup>-2</sup>; 18.08 °W, 19.15 °N) part of the CE and lowest values (26.8-  
368 37.5 mg m<sup>-2</sup>) in the eastern in the Southern (18.08 °W, 18 °N) and Eastern part (17.39 - 17.68  
369 °W, 18.58 °N). Depth distribution of Chl-*a* concentration also differed across the eddy, with  
370 values  $> 0.5$  µg L<sup>-1</sup> reaching down to 45 m depth at the Frontal Zone and the western part of the  
371 CE (19.11-19.55 °W) and down to 30 m depth in the eastern side of the CE (17.1-17.4 °W).  
372 Within the upper 30 m, Chl-*a* concentration within the CE was significantly higher than at the



373 open ocean and the coastal stations (ANOVA,  $p < 0.05$ ). Integrated autotrophic plankton  
 374 biomass ranged between 0.3 and 4.7 g C m<sup>-2</sup> in the CE (Table 1). Depth distribution of  
 375 autotrophic plankton biomass (Fig. 3b) showed low biomass in the upper 40 m (<25 μg C L<sup>-1</sup>)  
 376 from 18.83 to 19.11 °W. In contrast, higher biomass (>25 μg C L<sup>-1</sup>) occurred in the more eastern  
 377 stations of the CE (17.11 to 18.54 °W) and westwards from the Frontal Zone (19.55 °W). In the  
 378 eddy, autotrophic plankton biomass reached higher concentrations mostly within the upper 40  
 379 m, with values up to 191 μg C L<sup>-1</sup>. It should be noted that autotrophic biomass refers only to  
 380 pico- and nanophytoplankton and not to larger cells such as typical for diatoms or  
 381 dinoflagellates. Depth-integrated PP<sub>TOT</sub> and PP<sub>DOC</sub> rates were significantly higher in the CE and  
 382 at the Frontal Zone than at the open ocean and the coastal stations (Tukey,  $p < 0.05$ ) with values  
 383 ranging from 245 to 687 mmol C m<sup>-2</sup> d<sup>-1</sup> and from 95.9 to 238 mmol C m<sup>-2</sup> d<sup>-1</sup>, respectively  
 384 (Table 1). PP<sub>TOT</sub> rates (Fig. 2c; Table 2) were fairly constant across the CE's surface (5 m  
 385 depth), ranging between 11.7 to 13.3 μmol C L<sup>-1</sup> d<sup>-1</sup>, but varied strongly between 15-40 m depth  
 386 with values from 0.2 to 14.5 μmol C L<sup>-1</sup> d<sup>-1</sup>. The highest PP<sub>TOT</sub> rates were found in the Frontal  
 387 Zone with up to 25.0 μmol C L<sup>-1</sup> d<sup>-1</sup> at the surface. The range of PP<sub>DOC</sub> rates (Table 2) was  
 388 larger in the CE (0.2-4.9 μmol C L<sup>-1</sup> d<sup>-1</sup>) and the Frontal Zone (0.7-7.8 μmol C L<sup>-1</sup> d<sup>-1</sup>) than in  
 389 the open ocean and at the coastal stations. Integrated PER had a range of 29.4-43.3 % (Table  
 390 1). A slightly lower PER was observed within the upper 40 m (Fig. 2d) for the CE and Frontal  
 391 Zone compared to open ocean and coastal stations.

392

393 Table 1: Chlorophyll a (Chl *a*) and abundance, biomass and activity of phyto- and bacterial plankton,  
 394 integrated over the upper 100m depth. '-' indicate that the parameter was not measured. PP<sub>DOC</sub> and PP<sub>TOT</sub>  
 395 rates in St EDM-4E were measured on the 22/07/2019 from 5, 33 and 50m depth and CR and BR rates  
 396 were measured in St. E5 on the 29/07/2019 from 5, 35 and 50m depth.

Location	Station	Chl <i>a</i> (mg m <sup>-2</sup> )	AutPI (g C m <sup>-2</sup> )	PP <sub>DOC</sub> (mmol C m <sup>-2</sup> d <sup>-1</sup> )	PP <sub>TOT</sub> (mmol C m <sup>-2</sup> d <sup>-1</sup> )	PER (%)	HB (10 <sup>15</sup> cell m <sup>-2</sup> )	CR (mmol C m <sup>-2</sup> d <sup>-1</sup> )	BR (mmol C m <sup>-2</sup> d <sup>-1</sup> )	BP (mmol C m <sup>-2</sup> d <sup>-1</sup> )
Coastal	E5	54.5	6.1	75.2	137	54.9	14.7	99.6	32	2.9
	EDZ-10N	36.8	3.6	-	-	-	13.8	-	-	4.1
	AZM-3	58.7	5.3	-	-	-	12.9	-	-	5.7
Eddy Periphery	EDZ-8N	61.5	4.7	-	-	-	10.7	-	-	8.2
	EDZ-7N	26.8	1.6	-	-	-	9.4	-	-	5.7
	EDZ-6N	27.9	1.2	-	-	-	9.1	-	-	4.0
Eddy Core	EDZ-5N	39.2	4.1	-	-	-	14.5	154	59.1	4.7

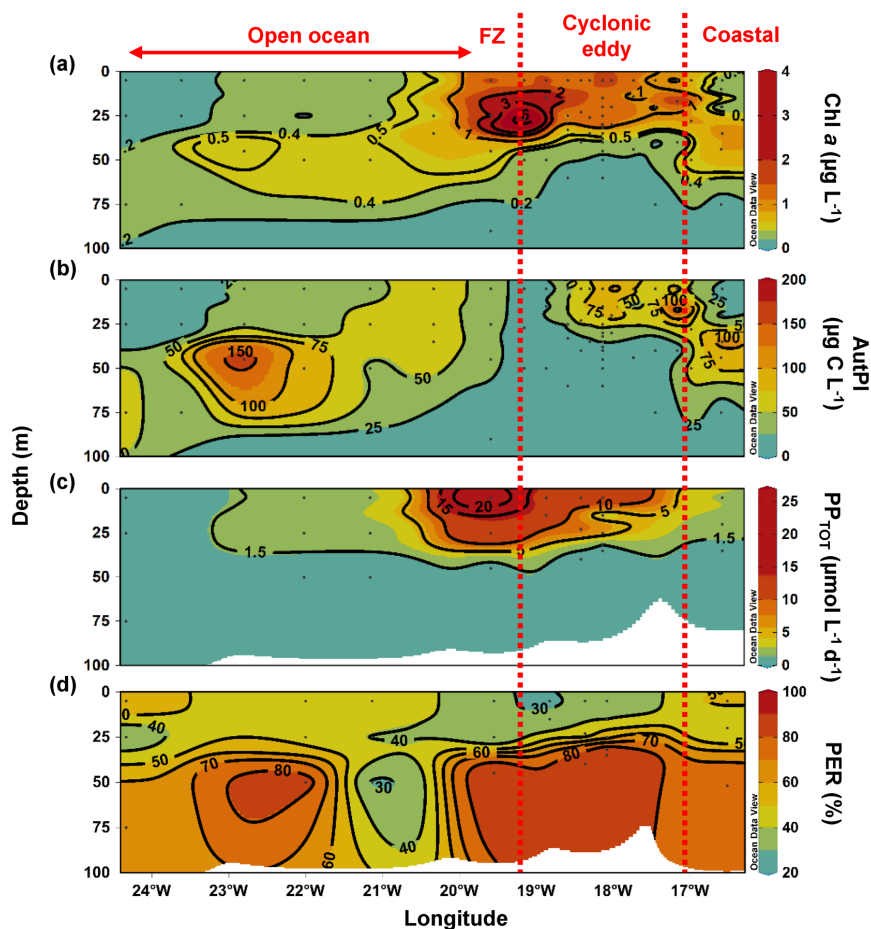


397 Table 1 cont.: Chlorophyll *a* (Chl *a*) and abundance, biomass and activity of phyto- and bacterial  
 398 plankton, integrated over the upper 100m depth. '-' indicate that the parameter was not measured. PP<sub>DOC</sub>  
 399 and PP<sub>TOT</sub> rates in St EDM-4E were measured on the 22/07/2019 from 5, 33 and 50m depth and CR and  
 400 BR rates were measured in St. E5 on the 29/07/2019 from 5, 35 and 50m depth.

Location	Station	Chl <i>a</i> (mg m <sup>-2</sup> )	AutPl (g C m <sup>-2</sup> )	PP <sub>DOC</sub> (mmol C m <sup>-2</sup> d <sup>-1</sup> )	PP <sub>TOT</sub> (mmol C m <sup>-2</sup> d <sup>-1</sup> )	PER (%)	HB (10 <sup>15</sup> cell m <sup>-2</sup> )	CR (mmol C m <sup>-2</sup> d <sup>-1</sup> )	BR (mmol C m <sup>-2</sup> d <sup>-1</sup> )	BP (mmol C m <sup>-2</sup> d <sup>-1</sup> )
Eddy Core	EDM-4E	46.0	3.3	95.9	245	39.2	15.2	135	60.8	4.5
	EDM-3E	77.5	3.2	-	-	-	15.3	-	-	8.6
	EDM-4	63.8	3.3	141	380	37.2	19.4	275	127	6.4
Eddy Periphery	S5	35.7	3.6	117	288	40.8	23.7	-	-	6.8
	EDM-5E	35.2	1.6	-	-	-	11.8	-	-	4.7
	EDM-2E	148	1.7	-	-	-	20.8	-	-	11.4
	EDZ-4	47.8	1.0	-	-	-	14.4	-	-	6.3
	EDZ-3	17.2	0.3	-	-	-	9.6	-	-	2.9
	EDZ-2	98.7	0.7	131	445	29.4	8.2	592	320	8.1
	EDZ-1	225	0.6	-	-	-	13.7	-	-	19.3
Frontal Zone	E3	72.1	2.4	238	687	34.6	12.9	529	257	7.7
Open ocean	S4	40.2	4.5	-	-	-	16.9	-	-	4.3
	S3	30.7	4.0	42.8	101	42.3	14.5	346	148	2.6
	E2	22.3	4.4	78.0	116	67.5	12.2	387	168	2.3
	S2	34.1	7.8	-	-	-	13.9	-	-	2.1
	S1	12.2	1.6	-	-	-	5.4	-	-	0.7
	E1	11.7	2.3	12.3	25.8	47.6	6.7	19.7	6.3	0.8

401





402

403 Figure 3: Depth distribution of phytoplankton biomass and activity over 100m depth: Chlorophyll *a* (Chl  
404 *a*; **a**), Autotrophic plankton biomass (AutPI; **b**), total primary production (PP<sub>TOT</sub>; **c**), and percentage of  
405 extracellular release (PER; **d**). Red dashed line show the eddy-influenced area and FZ refer as Frontal  
406 Zone.

407

### 408 3.3 Bacterial abundance and activities

409 Heterotrophic bacterial abundance decreased with depth and was highest in the upper 50 m of  
410 all stations (Fig. 4a). At the coastal and open ocean stations, integrated (0-100 m depth)  
411 heterotrophic bacteria abundance ranged between 12.9-14.7 and 5.4-16.9x10<sup>15</sup> cells m<sup>-2</sup>,  
412 respectively (Table 1). No significant differences in heterotrophic bacterial abundance were  
413 observed between the open ocean and coastal stations (Tukey,  $p>0.05$ ). In the open ocean



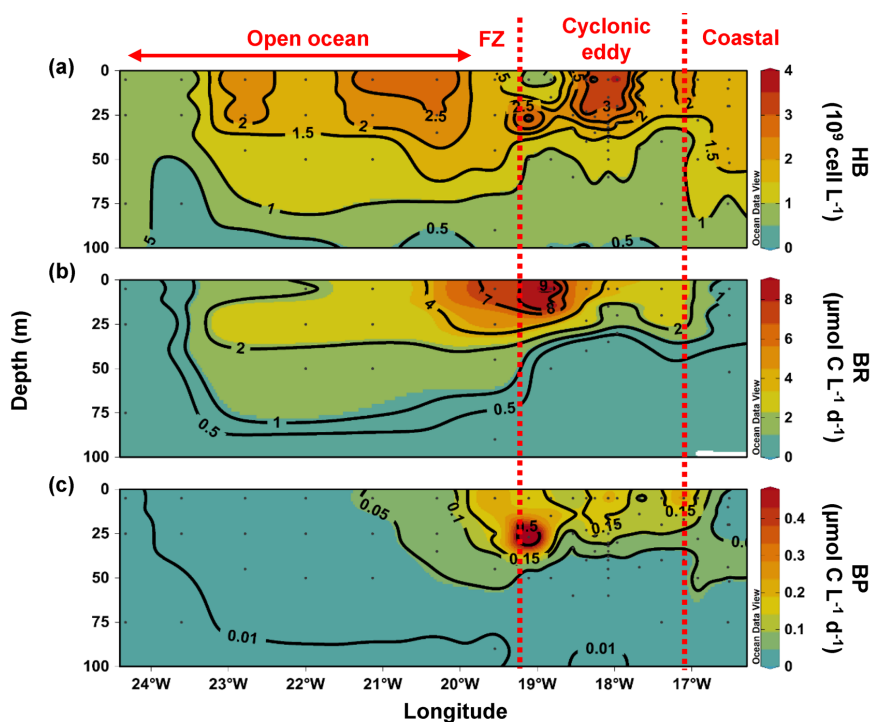
414 waters, the lowest integrated BR and CR rates (Table 1) were reported at the station furthest  
415 offshore (24.33 °W), with 6.3 and 19.7 mmol C m<sup>-2</sup> d<sup>-1</sup>, respectively. Yet in the other open  
416 ocean stations (21.13 to 22 °W), integrated BR and CR rates were higher (148-168 and 346-  
417 348 mmol C m<sup>-2</sup> d<sup>-1</sup> respectively) than in the coastal station (32 and 98 mmol C m<sup>-2</sup> d<sup>-1</sup>  
418 respectively). Overall, BR and CR rates were higher in the open ocean than at the coastal  
419 stations with high rates (> 1 and > 2.5 μmol C L<sup>-1</sup> d<sup>-1</sup>, respectively) down to 60 m depth (Fig.  
420 **4b**; SI Fig. **S5a**). Integrated BP, in contrast, was generally higher at the coastal stations with  
421 2.9-5.7 mmol C m<sup>-2</sup> d<sup>-1</sup> compared to the open ocean with 0.7-4.3 mmol C m<sup>-2</sup> d<sup>-1</sup> (Table 1).  
422 However, BP rates were not significantly different from the open ocean (Tukey  $p > 0.05$ ), where  
423 BP rates were more variable. At the coastal stations, the highest BP (Fig. **4b**) rates were  
424 observed at the surface (5 m) and around ~40 m depth, while in the open ocean, the highest  
425 rates were found at the surface (5 m). BGE was determined for the upper 50 m (Table 2) and  
426 showed only little variability over depth. However, BGE was significantly higher (Tukey,  $p <$   
427  $0.05$ ) at the coastal than at the open ocean stations with ranges of  $5.3 \pm 2.2$  to  $8.0 \pm 1.0\%$   
428 compared to  $0.9 \pm 0.04$  to  $2.3 \pm 0.02\%$ , respectively. We estimated the predominance of  
429 autotrophy/heterotrophy in the system, by dividing the PP<sub>TOT</sub> rates by the BCD. Heterotrophic  
430 conditions ( $\frac{PP_{TOT}}{BCD} < 1$ ) occurred at the open ocean stations throughout the water column, while  
431 autotrophic conditions ( $\frac{PP_{TOT}}{BCD} > 1$ ) prevailed at the coastal St. E5 (Table 2). This pattern was  
432 preserved when data were integrated over the mixed layer (Fig. 5) apart for the furthest station  
433 offshore (24.33 °W) where autotrophy occurred, yet lower than at the coastal station St.E5  
434 ( $\frac{PP_{TOT}}{BCD} = 2$  and 5.5 respectively). PP<sub>DOC</sub> rates were sufficient to satisfy the BCD at the coastal  
435 St.E5 but not in the open ocean stations (Table 2).

436 In the CE and at the Frontal Zone, integrated heterotrophic bacterial abundance ranged from  
437  $8.2 - 23.7 \times 10^{15}$  cells m<sup>-2</sup> (Table 1). In the CE, substantial variation of bacterial abundance  
438 occurred within the upper 20 m (Fig. **4a**), with an abundance of  $< 1 \times 10^9$  cells L<sup>-1</sup> in the western  
439 CE periphery (18.83 to 19.11 °W) and  $> 3 \times 10^9$  cells L<sup>-1</sup> in the CE core stations (~18 °W).  
440 Depth-integrated BR and CR (Table 1) ranged between 59.1 and 320 and between 135 and 592  
441 mmol C m<sup>-2</sup> d<sup>-1</sup>, respectively. Elevated BR and CR rates (> 1 and 2.5 μmol C L<sup>-1</sup> d<sup>-1</sup>,  
442 respectively) were only present in the upper ~30-40 m of the CE (Fig. **4b**; SI Fig. **S5a**).  
443 Integrated BP rates ranged from 2.9 to 19.3 mmol C m<sup>-2</sup> d<sup>-1</sup> in the CE and at the Frontal Zone  
444 stations (Table 1). BP rates in the upper 40 m of the CE and at the Frontal Zone were elevated  
445 but were significantly higher than in the coastal and open ocean stations only in the stations



446 within the CE periphery (Tukey  $p < 0.05$ ). Stations in the core of the CE had BGEs (Table 2)  
447 significantly higher than the stations located in the open ocean (Tukey,  $p < 0.05$ ). BGE had a  
448 range of  $1.4 \pm 2.2$  to  $10.5 \pm 0.5$  % and  $2.8 \pm 0.1$  to  $3.0 \pm 1.7$  % in the CE and the Frontal Zone  
449 stations, respectively. Highest BGE was observed below 20 m depth in the CE core (up to  
450 10.48%, St EDM-4E). With ratios ranging from 1.13 to 3.5, the upper 40 m of the CE and the  
451 Frontal Zone stations were rather autotrophic (Table 2). When integrated over the mixed layer  
452 (Fig. 5), stations within the CE and at the Frontal Zone were autotrophic, with a  $\frac{PP_{TOT}}{BCD}$  ratio  
453 ranging from 1.17 to 3.8.  $PP_{DOC}$  was on average 70% of the BCD within the CE and the Frontal  
454 Zone, yet ranging from 28.3 to 114.5%.

455



456  
457 Figure 4: Depth distribution of bacterial abundance and microbial activities over 100m depth:  
458 Heterotrophic bacterial abundance (HB; a), bacterial respiration (BR; b), bacterial production (BP; c).  
459 Red dashed line show the eddy-influenced area and FZ refers to Frontal Zone.

460

461



462 Table 2: Average (mean) ± standard deviation of microbial metabolic activities during M156: bacterial  
 463 carbon demand (BCD); bacterial growth efficiency (BGE); dissolved primary production (PP<sub>DOC</sub>);  
 464 Percentage of extracellular release (PER); total primary production (PP<sub>TOT</sub>) and the ratio between BCD  
 465 and PPTOT ( $\frac{BCD}{PP_{TOT}}$ ). BCD and BGE were obtained from BP and BR rates at 22°C (see text). ‘-‘ indicate  
 466 that the parameter was not measured and B.D. below detection (see text). PP<sub>DOC</sub> and PP<sub>TOT</sub> rates in St.  
 467 EDM-4E were measured on the 22/07/2019 from 5, 33 and 50m depth and CR and BR rates were  
 468 measured in St. E5 on the 29/07/2019 from 5, 35 and 50m depth.

Location	Station	Depth (m)	BCD ( $\mu\text{mol C L}^{-1} \text{d}^{-1}$ )	BGE (%)	PP <sub>DOC</sub> ( $\mu\text{mol C L}^{-1} \text{d}^{-1}$ )	PER (%)	PP <sub>TOT</sub> ( $\mu\text{mol C L}^{-1} \text{d}^{-1}$ )	$\frac{BCD}{PP_{TOT}}$
Coastal	E5	5	0.6 ± 0.1	5.3 ± 2.2	1.5 ± 0.2	34.9 ± 1.1	2.7 ± 0.2	4.5 ± 1.5
		20	0.5 ± 0.1	6.9 ± 1.6	1.2 ± 0.1	52.6 ± 2.7	2.5 ± 0.1	5.5 ± 1.4
		35	0.5 ± 0.3	8.0 ± 1.0	0.7 ± 0.1	89.8 ± 3.9	1.0 ± 0.1	2.1 ± 0.2
Eddy Periphery	EDZ-10N	All	-	-	-	-	-	-
	S6	All	-	-	-	-	-	-
	EDZ-8N	All	-	-	-	-	-	-
	EDZ-7N	5	3.5 ± 0.7	3.6 ± 0.3	-	-	-	-
		20	3.5 ± 0.3	3.3 ± 1.7	-	-	-	-
	EDZ-6N	All	-	-	-	-	-	-
Eddy Core	EDZ-5N	5	2.6 ± 0.4	6.02 ± 1.5	-	-	-	-
		20	1.15 ± 0.3	9.51 ± 2.1	-	-	-	-
		30	0.41 ± 0.6	7.11 ± 0.2	-	-	-	-
		100	B.D.	B.D.	-	-	-	-
EDM-4E	EDM-4E	5	4.5 ± 0.4	4.1 ± 1.1	4.3 ± 0.1	36.7 ± 0.2	11.2 ± 0.1	2.5 ± 0.2
		15	1.3 ± 0.4	10.5 ± 0.6	0.4 ± 0.1	39.3 ± 6.8	1.1 ± 0.1	2.1 ± 0.4
		35	B.D.	B.D.	0.6 ± 0.3	94.4 ± 0.9	0.6 ± 0.3	-
		60	B.D.	B.D.	-	-	-	-
		EDM-3E	All	-	-	-	-	-
EDM-4	EDM-4	5	4.7 ± 1.1	3.2 ± 1.4	4.3 ± 1.0	35.1 ± 5.7	12.6 ± 1.2	2.7 ± 1.1
		23	3.4 ± 0.2	4.4 ± 2.1	3.9 ± 0.2	35.7 ± 1.4	11.0 ± 0.3	3.2 ± 1.4
		40	B.D.	B.D.	0.3 ± 0.1	85.3 ± 7.1	0.3 ± 0.1	-
		100	B.D.	B.D.	-	-	-	-
Eddy Periphery	S5	5	-	-	4.8 ± 0.4	34.9 ± 1.1	13.7 ± 0.7	-
		25	-	-	3.4 ± 0.3	52.6 ± 2.7	6.5 ± 0.4	-
		32	-	-	0.2 ± 0.1	89.8 ± 3.9	0.2 ± 0.1	-

469

470



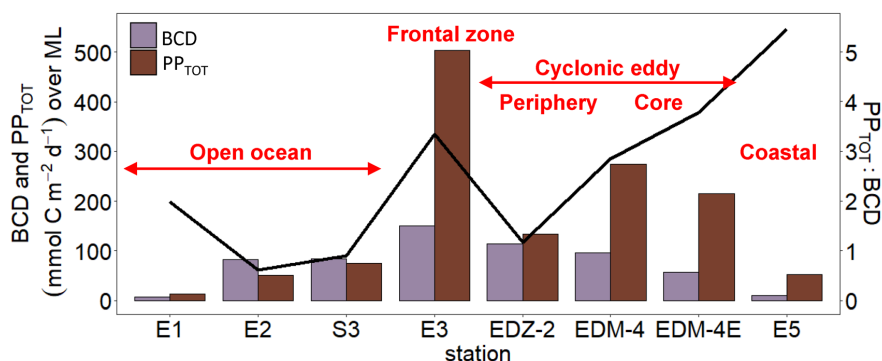
471 Table 2 cont.: Average (mean) ± standard deviation of microbial metabolic activities during M156:  
 472 bacterial carbon demand (BCD); bacterial growth efficiency (BGE); dissolved primary production  
 473 (PP<sub>DOC</sub>); Percentage of extracellular release (PER); total primary production (PP<sub>TOT</sub>) and the ratio  
 474 between BCD and PPTOT ( $\frac{BCD}{PP_{TOT}}$ ). BCD and BGE were obtained from BP and BR rates at 22°C (see  
 475 text). ‘-’ indicate that the parameter was not measured and B.D. below detection (see text).

Location	Station	Depth (m)	BCD (μmol C L <sup>-1</sup> d <sup>-1</sup> )	BGE (%)	PP <sub>DOC</sub> (μmol C L <sup>-1</sup> d <sup>-1</sup> )	PER (%)	PP <sub>TOT</sub> (μmol C L <sup>-1</sup> d <sup>-1</sup> )	$\frac{BCD}{PP_{TOT}}$
Eddy Periphery	EDM-5E	All	-	-	-	-	-	-
	EDM-2E	All	-	-	-	-	-	-
	EDZ-4	All	-	-	-	-	-	-
	EDZ-3	All	-	-	-	-	-	-
	EDZ-2	5	10.5 ± 0.5	1.4 ± 2.2	2.9 ± 0.3	25.1 ± 3.4	11.9 ± 1.0	2.1
		15	9.4 ± 2.3	2.5 ± 0.7	4.9 ± 0.1	31.0 ± 1.7	14.5 ± 0.6	0.3
		50	B.D.	B.D.	-	-	-	-
100		B.D.	B.D.	-	-	-	-	
EDZ-1	All	-	-	-	-	-	-	
Frontal Zone	E3	5	7.1 ± 0.4	3.0 ± 1.7	7.8 ± 0.4	31.7 ± 1.7	25.0 ± 0.9	3.5 ± 2.2
		25	4.8 ± 1.1	2.8 ± 0.1	5.0 ± 0.6	33.4 ± 3.2	14.3 ± 0.8	3.0 ± 0.7
		45	1.9 ± 0.6	2.9 ± 2.1	0.7 ± 0.2	87.0 ± 3.3	0.8 ± 0.2	0.4 ± 0.3
		90	B.D.	B.D.	-	-	-	-
Open ocean	S4	All	-	-	-	-	-	-
	S3	5	3.2 ± 0.5	1.6 ± 0.2	1.3 ± 0.2	49.1 ± 5.5	2.7 ± 0.3	0.9 ± 0.5
		25	2.6 ± 0.5	1.7 ± 1.1	1.16 ± 0.03	38.4 ± 0.9	2.5 ± 0.03	1.0 ± 0.3
		50	1.2 ± 1.1	1.8 ± 0.2	0.0 ± 0.01	21.8 ± 6.6	0.1 ± 0.01	0.1 ± 0.1
		100	B.D.	B.D.	-	-	-	-
	E2	5	1.8 ± 0.6	1.8 ± 0.2	0.6 ± 0.1	40.9 ± 3.4	1.38 ± 0.1	0.8 ± 0.1
		25	3.5 ± 1.1	0.9 ± 0.04	0.94 ± 0.1	50.2 ± 3.1	1.89 ± 0.1	0.5 ± 0.1
		50	1.7 ± 0.4	1.6 ± 0.4	1.25 ± 0.3	91.3 ± 2.5	1.4 ± 0.3	0.8 ± 0.8
		100	B.D.	B.D.	-	-	-	-
	S2	All	-	-	-	-	-	-
	S1	All	-	-	-	-	-	-
	E1	5	0.4 ± 0.2	2.3 ± 0.02	0.23 ± 0.1	54.7 ± 13.3	0.39 ± 0.1	0.9 ± 0.5
		25	B.D.	B.D.	0.18 ± 0.01	38.5 ± 0.6	0.43 ± 0.01	-
75		B.D.	B.D.	0.08 ± 0.02	61.7 ± 6.2	0.13 ± 0.02	-	
125		B.D.	B.D.	-	-	-	-	

476



477



479

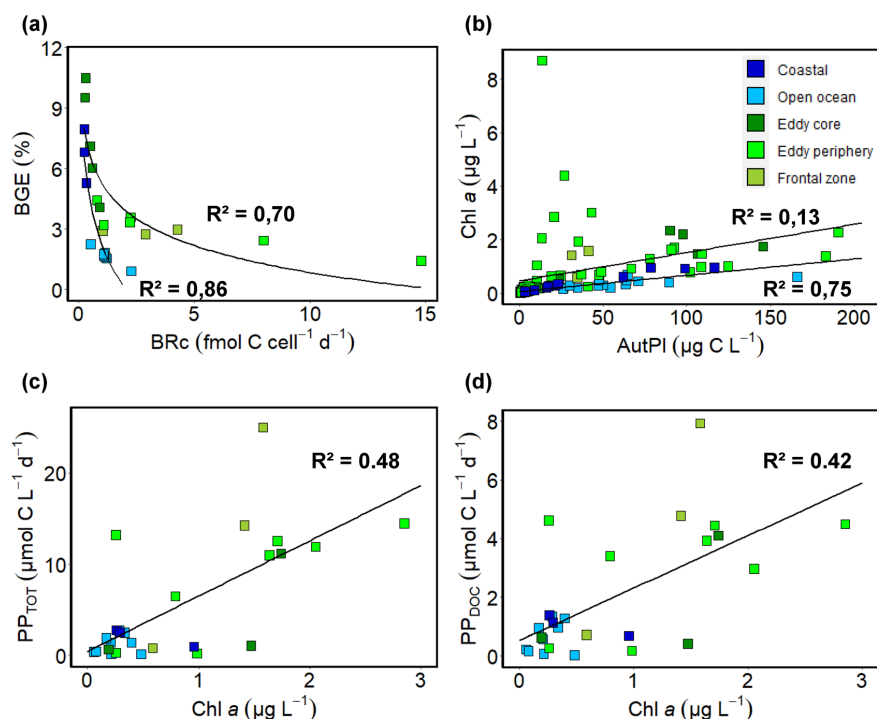
480 Figure 5: Integrated total primary production (PP<sub>TOT</sub>) and bacterial carbon demand (BCD) rates over the  
481 mixed layer during M156. Blackline reports the ratio between PP<sub>TOT</sub> and BCD. More information are  
482 given in SI table 1.

483

### 484 3.4 Indices of phyto- and bacterioplankton activity change

485 We investigated the impact of the CE on heterotrophic bacterial and phytoplankton abundance  
486 by regression analysis of, cell-specific BR and BGE (Fig. 6a), as well as autotrophic plankton  
487 biomass and Chl-*a* (Fig. 6b). We noticed a negative semilogarithmic relationship (Fig. 6a)  
488 between cell-specific BR rates and the BGE in both the zonal transect (coastal+open ocean)  
489 [BG= -3.11 ln (cell-specific BR) + 2.35; R<sup>2</sup>=0.86; *p*<0.001] and the eddy influenced region (CE  
490 + Frontal Zone) [BGE= -1.92 ln (cell-specific BR) + 5.28; R<sup>2</sup>=0.70; *p*=0.001]. Concerning the  
491 phytoplankton (Fig. 6b), we observed that Chl-*a* and autotrophic plankton biomass were  
492 linearly correlated in the open ocean and coastal region (R<sup>2</sup>=0.75; *p*<0.001) while being poorly  
493 correlated in the CE-influenced area (R<sup>2</sup>=0.13).

494



495

496 Figure 6: Relationship between (a) cell-specific bacterial respiration (BRc) and bacterial growth  
497 efficiency (BGE), (b) chlorophyll *a* (Chl *a*) and autotrophic plankton biomass (AutPI), (c) total primary  
498 production (PP<sub>TOT</sub>) and Chl *a* and (d) dissolved primary production (PP<sub>DOC</sub>) and Chl *a*. Black lines in  
499 (a) and (b) show regression from the open ocean and coastal stations (blue shades) and from the stations  
500 in eddy influenced area (green shades). Black lines in (c) and (d) show regressions in all the stations.

501

### 502 3.5 Semi-labile dissolved organic carbon

503 Between coastal and open ocean stations, SL-DOC concentration was not significantly different  
504 (Tukey,  $p > 0.05$ ; SI Fig. S5b) with ranges of 1.9-8.0  $\mu\text{mol L}^{-1}$  and 4.7-18.9  $\mu\text{mol L}^{-1}$ ,  
505 respectively. At those sites, SL-DOC distribution was rather uniform in the upper 40 m with  
506 SL-DOC  $> 5 \mu\text{mol L}^{-1}$ , apart from the station furthest offshore from 22.7-24.3 °W where SL-  
507 DOC  $> 5 \mu\text{mol L}^{-1}$  was limited to shallow depth (5 m). In the CE and at the Frontal Zone, SL-  
508 DOC concentration was clearly elevated and increased from East to West with an overall range  
509 of 1.4-54.3  $\mu\text{mol L}^{-1}$ . At the Frontal Zone, SL-DOC concentration  $> 5 \mu\text{mol L}^{-1}$  was detectable  
510 down to 90 m depth.

511



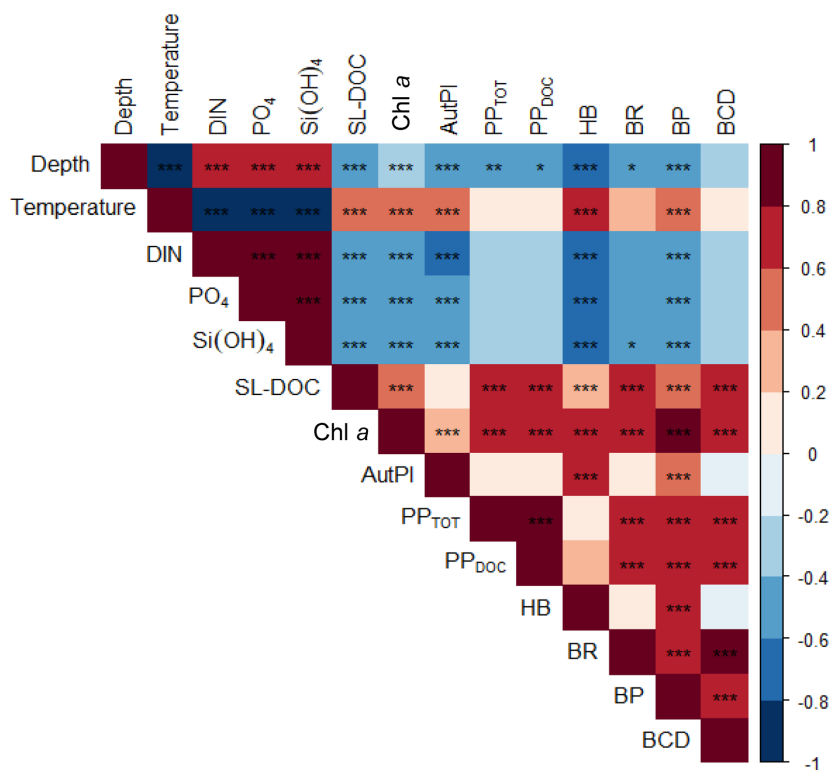


512 3.6 Correlation analysis

513 We applied a Pearson correlation matrix (Fig. 7) to reveal significant correlations between the  
514 measured parameters. Temperature correlated negatively with nutrients (DIN, PO<sub>4</sub>, Si(OH)<sub>4</sub>;  
515 Pearson,  $R < -0.9$ ,  $p < 0.001$ ) and positively with bacteria (Pearson,  $R = 0.65$ ,  $p < 0.001$ ). Total  
516 (PP<sub>TOT</sub>) and dissolved primary production (PP<sub>DOC</sub>) were positively correlated to each other  
517 (Pearson,  $R = 0.98$ ,  $p < 0.001$ ) and to Chl-*a* and SL-DOC (Pearson,  $R > 0.65$  and  $> 0.60$   
518 respectively,  $p < 0.001$ ), but not to the autotrophic plankton biomass (Pearson,  $R < 0.14$ ,  $p > 0.05$ ).  
519 Bacterial biomass production (BP) and respiration (BR) were positively correlated (Pearson,  
520  $R = 0.78$ ,  $p < 0.001$ ). BCD was more correlated to BR than to BP (Pearson,  $R = 1$  and  $R = 0.74$   
521 respectively,  $p < 0.001$ ). A clear coupling between phytoplankton and bacteria was indicated, by  
522 positive correlations between PP<sub>TOT</sub> and PP<sub>DOC</sub> and BP, BR, and BCD (Pearson,  $R > 0.70$ ,  
523  $p < 0.001$ ), BP and Chl-*a* (Pearson,  $R = 0.93$ ,  $p < 0.001$ ), and BR and Chl-*a* and the SL-DOC  
524 concentration (Pearson,  $R = 0.78$  and  $0.75$  respectively,  $p < 0.001$ ).

525

526



527

528 Figure 7: Correlations of biochemical parameters, metabolic activities, and bacterial abundance in the  
 529 upper 200 m during M156. Colour scale: correlation coefficient (r). Statistical significance: ‘\*\*\*’ <  
 530 0.001, ‘\*\*’ < 0.01, ‘\*’ < 0.05.

531

## 532 4. Discussion

533

534 4.1 Distribution of phytoplankton abundance and activity in the Mauritanian upwelling  
 535 system associated with cyclonic eddy perturbation

536

537 In general, coastal Chl-*a* concentration during this study was not as high as observed in earlier  
 538 studies with strong coastal upwelling (e.g. Alonso-Sáez et al., 2007; Agustí and Duarte, 2013;  
 539 Arístegui et al., 2020). This might be related to the relatively weak upwelling, as a result of  
 540 weak surface winds along the Mauritanian Coast typically occurring during summer when our  
 541 samples were collected (Peligrí and Peña-Izquierdo, 2015a). Consequently, during summer,



542 fewer nutrients reach the euphotic zone by coastal upwelling, while offshore surface wind  
543 remains strong and might enhance vertical mixing at the surface. Coastal Chl-*a* concentration  
544 was only slightly higher compared to the open ocean, and both the coastal and open ocean  
545 phytoplankton communities were dominated by cells <20µm, as indicated by the strong linear  
546 correlation between Chl-*a* and autotrophic plankton biomass (Fig. 6b).

547 We did not observe a marked gradient in phytoplankton productivity either, unlike other regions  
548 of the CanUS with permanent upwelling conditions (Demarcq and Somoue, 2015; Arístegui et  
549 al., 2020). PP<sub>TOT</sub> rates stayed rather constant from the coast to the open ocean and were in the  
550 range of reported rates in oligotrophic offshore waters of the CanUS (Agustí and Duarte, 2013;  
551 Lasternas et al., 2014). SL-DOC was relatively constant as well, with variations attributable to  
552 the westward propagation of the currents and eddies (SI Fig. S5b; Lovecchio et al., 2017, 2018).  
553 The absence of upwelling and the dominance of small autotrophic cells (<20µm) in the  
554 phytoplankton community suggest that in the open ocean and coastal stations, primary  
555 productivity was maintained through remineralisation of nutrients released from dying cells.  
556 Indeed, plankton mortality rates have been reported to increase with decreasing cell size (Marbá  
557 et al., 2007) and with increasing PER (Lasternas et al., 2014). Agustí and Duarte (2013) reported  
558 PER to range from ~1% in ‘healthy’ communities from the upwelled waters of the CanUS to  
559 ~70% in ‘dying’ communities from the oligotrophic waters of the ETNA. PER in our study was  
560 on average  $51.1 \pm 17\%$  in the open ocean and coastal stations leading to the conclusion that  
561 primary productivity in those areas was maintained mainly through remineralisation of small  
562 (<20µm) plankton cells.

563 The CE broke this rather uniform distribution of phytoplankton productivity and community  
564 through coastal and open ocean waters. From a depth distribution perspective, Chl-*a* isolines  
565 seemed to have been pushed toward the surface in the CE (Fig. 3a). Similar ‘compression’ of  
566 Chl-*a* isolines towards the surface have been reported in eddies earlier (Lochte and Pfannkuche  
567 1987; Feng et al., 2007; Noyon et al., 2019). Such compressions have been attributed to  
568 resulting from phytoplankton growth through upwelling of nutrients combined with high  
569 vertical mixing from strong surface winds, which favour phytoplankton distribution at the  
570 surface (Feng et al., 2007; Noyon et al., 2019). In the CE, the upwelling was marked by the  
571 hydrographic parameters (e.g. temperature, salinity, nutrients, Fig. 2), and before the eddy  
572 survey, strong surface winds occurred offshore (SI Fig. S7). Therefore, the phytoplankton  
573 which grew from upwelled nutrients must have been relocated to the surface through mixing,



574 the reason why high Chl-*a* ( $>0.5 \mu\text{g L}^{-1}$ ) concentration was found at the surface (5m) in all  
575 stations within the CE.

576 In addition, Chl-*a* was dispatched differently within the CE with the highest concentrations in  
577 the Western and Northern part and lowest concentrations in the Southern and Eastern part  
578 (Table 1; SI Fig. S4). Furthermore, an almost continuous deepening of high Chl-*a* ( $>0.5 \mu\text{g L}^{-1}$ )  
579 distribution, as well as an increase of SL-DOC concentration, was observed in the CE from  
580 East to West (Fig. 3a; SI Fig. S5b). Chelton et al. (2011) established from satellite observation  
581 and an eddy-centric perspective that due to the rotational flow and the westward propagation of  
582 CEs Chl-*a* tends to accumulate in their Southwest quadrants while being lower in their  
583 Northeast quadrants. Since in our case, the CE shape was elliptic, we assume that the rotational  
584 flow in the CE changed, shifting the accumulation. To the best of our knowledge, this is the  
585 first time that high-resolution sampling could demonstrate this specific submesoscale Chl-*a*  
586 distribution within a CE.

587 Outside of the CE boundaries, we noticed a thermal front with colder surface water. Thermal  
588 fronts are often detected out of eddies periphery as a consequence of eddy-eddy interaction (See  
589 review by Mahadevan, 2016) and/or eddy-wind interaction (Xu et al., 2019). In this Frontal  
590 Zone, we observed higher nutrient content than the adjacent stations and a doming of the  
591 nutriclines marking an upwelling (Fig. 2a, d-f). Thus, Chl-*a* was elevated, and ‘compressed’ to  
592 the surface similarly as in the CE (Fig. 3a). We assume this distribution to be the consequence  
593 of the same factors affecting the CE (upwelling, mixing induced by strong surface winds).

594 In the CE-influenced area (CE+Frontal Zone), Chl-*a* concentration was disconnected from  
595 small ( $<20\mu\text{m}$ ) autotrophic plankton biomass (Fig. 6b). This implies that in the West of the  
596 eddy where Chl-*a* was high and small autotrophic plankton biomass low (Fig. 3a & b), larger  
597 autotrophic cells such as diatoms and/or dinoflagellate were present in higher quantities. We  
598 corroborate this point from lipid biomarkers concentration (unpublished data) as fucoxanthin,  
599 a typical marker of diatoms (Stauber and Jeffrey, 1998), was the dominant pigment in the  
600 Western part of the CE. This is consistent with previous studies in which CEs unevenly altered  
601 the phytoplankton community, often reporting the presence of diatoms/dinoflagellates (e.g.,  
602 Lochte and Pfannkuche, 1987; Lasternas et al., 2013). The details of autotrophic plankton  
603 composition (SI Fig. S7) confirm this diversity, with the uneven distribution of cyanobacteria  
604 (*Synechococcus*) and eukaryotic pico- and nanoplankton within the CE underscoring the fact  
605 that the phytoplankton community was likely separate from the transect and diverse within a  
606 submesoscale range.



607 Therefore, the CE dispatched different phytoplankton taxa with different potentials of primary  
608 production and resources acquisition. Moreover, the mixed layer was also highly variable  
609 within the CE leading to substantial variation of  $PP_{TOT}$  rates (SI Table 1, Figure 5). Hence, we  
610 observed a three-fold variation of depth-integrated  $PP_{TOT}$  rates over 100m depth (Table 1)  
611 within the CE which is coherent with earlier observations of a fivefold variation of primary  
612 production integrated over the euphotic zone in a CE in the subtropical Pacific Ocean  
613 (Falkowski et al., 1991). Overall, primary productivity was enhanced within the CE and the  
614 Frontal Zone with an average of fourfold more depth-integrated  $PP_{TOT}$  rates over 100m depth  
615 than in the open ocean and coastal stations. This is coherent with Löscher et al. (2015) who  
616 found that depth-integrated primary productivity over the chlorophyll *a* maximum of a CE in  
617 the Mauritanian upwelling system was threefold higher than the surrounding waters. Exudation  
618 rates ( $PP_{DOC}$ ) were also enhanced within the eddy and integrated (0-100 m)  $PP_{DOC}$  rates were  
619 on average three-fold time higher than in the transect (Table 1). Yet, even if  $PP_{DOC}$  rates were  
620 higher within the CE and at the Frontal Zone stations (Table 2), PER was slightly lower at the  
621 surface (Fig. 3d). We start from two hypotheses regarding this distribution 1) the lower PER  
622 reported was due to a higher proportion of larger phytoplankton (e.g. diatoms) who have lower  
623 turnover rates and therefore have lower PER and/or 2) the upwelling of nutrients generated by  
624 the CE might have enhanced the physiological health of the phytoplankton community (Agustí  
625 and Duarte, 2013; Laternas and Agustí, 2014).

626

#### 627 4.2 Heterotrophic bacteria abundance and activities responses in the Mauritanian 628 upwelling system

629

630 Along the zonal transect (open ocean+coastal stations), a strong coupling between HB  
631 abundance and  $PP_{TOT}$  rates was observed ( $R^2=0.72$ ). Therefore, HB abundance followed the  
632 same trends as the  $PP_{TOT}$  by being continuously distributed from the coast to the offshore  
633 waters. Bachmann et al. (2018) reported a similar trend in the Mauritanian upwelling system  
634 during summer, strengthening our finding.

635 Bacterial activities were distributed differently. Both BR and BP were within the range of  
636 reported rates for coastal and offshore water of the CanUS (Reinthal et al., 2006; Alonso-  
637 Saez et al., 2007; Vaqué et al., 2014). BP rates slightly decreased from the coast to the open  
638 ocean. Similar trends were found in the CanUS with different upwelling intensities and at



639 different seasons (Alonso-Saez et al., 2007; Vaqué et al., 2014). Therefore, those factors  
640 (upwelling intensity and seasonality) were likely only indirectly coupled with BP variability,  
641 which instead was rather driven by the composition of the phytoplankton community. Indeed,  
642 BP was more correlated to Chl-*a* than autotrophic plankton biomass (<20µm; Fig. 7) suggesting  
643 that BP was more enhanced by the presence of larger autotrophic cells, such as diatoms or  
644 dinoflagellates. Those have larger phycospheres allowing them to attract more bacteria by  
645 chemotaxis (see review by Seymour et al., 2017). Hence, bacteria may benefit from mutualistic  
646 relationships with larger algae increasing their BP. Fucoxanthin, was decreasing from the  
647 coastal to offshore waters with overall low relative abundance (5-15%) (data not shown). Being  
648 part of microphytoplankton, especially diatoms have higher viability in coastal than in offshore  
649 waters of the CanUS (Lasternas et al., 2013), which may explain the observed fucoxanthin  
650 gradient.

651 In contrast, BR rates were higher in offshore than in coastal waters. BR rates were coupled to  
652 SL-DOC concentration, which is in agreement with Xu et al. (2013), who also found BR to be  
653 enhanced by low molecular weight DOC compound (<30kDa). SL-DOC compounds have a  
654 turnover of weeks to months, which allows them to escape rapid microbial degradation (Hansell  
655 et al., 2009). In the CanUS, currents and eddies can laterally transport DOC up to 2000 km  
656 (Lovecchio et al., 2018). Hence, we state that SL-DOC compounds produced at the coast have  
657 been relocated offshore while being slowly respired by heterotrophic bacteria along the way.

658 The distinct distribution of BP and BR rates affected the distribution of the BGE, which was  
659 higher in the coastal than in the open ocean stations. This is in accordance with observations by  
660 Alonso-Sáez et al. (2007) who showed higher BGE in the upwelling area above Cape Blanc  
661 than in the offshore waters of the CanUS. Overall, the BGEs reported here are among the lowest  
662 reported with all values <11%, but not surprising since BGE is negatively correlated to  
663 temperature and, therefore, reduced in the tropical ocean (Rivkin and Legendre, 2001). Yet we  
664 report an average BGE three times lower than Alonso-Sáez et al., (2007). We assume this  
665 difference to result from the difference in upwelling intensity (none vs. permanent). Indeed,  
666 Kim et al. (2017) denoted that BGE increased with increasing upwelling intensity in the Ulleung  
667 Basin. Under none or low upwelling conditions, bacteria compete with phytoplankton for  
668 nutrient acquisition. Moreover, as microphytoplankton do not thrive in the water column due  
669 to their high nutrient requirements (see review by Marañón, 2015), bacteria benefit less from  
670 their phycospheres. Hence, we expect BP to be lower in the relaxation period (May to July)



671 post upwelling than in the upwelling season (January to March; Lathuilière et al., 2008) in the  
672 Mauritanian upwelling system.

673 Within the CE-influenced stations (CE + Frontal Zone), HB abundance was disconnected from  
674 the  $PP_{TOT}$  rates (Fig. 4a). HB abundance was significantly higher in the core of eddy but  
675 surprisingly low at the Southwestern side of the eddy periphery (18.83 to 19.11 °W), where  
676 both  $PP_{TOT}$  rates and Chl-*a* were high (Fig. 3a, c). Hernández-Hernández et al. (2020) reported  
677 a similar feature with a strong disparity of HB biomass distribution within a CE in the CanUS.  
678 Since Chl-*a* and SL-DOC compounds accumulated in the Southwestern part of the CE, gel-  
679 likes particles produced by phytoplankton and bacteria such as transparent exopolymer particles  
680 (TEP) (Passow, 2002) might have also accumulated there. We hypothesize that a missing  
681 fraction of the bacteria might have been attached to gel-like particles (Busch et al., 2018) or  
682 other particulate matter.

683 The BP was particularly stimulated within the CE-influenced stations and on average threefold  
684 higher than in the open ocean stations when integrated over 100 m. This is in accordance with  
685 earlier studies from the Sargasso Sea (Ewart et al., 2008), the CanUS (Baltar et al., 2010), and  
686 in the Mediterranean Sea (Belkin et al., 2022) where CEs enhanced BP. As stated previously,  
687 the upwelling induced by the CE and the Frontal Zone led to higher phytoplankton biomass,  
688 including diatoms and/or dinoflagellates which were likely responsible for this increase in BP.

689 BR rates were also enhanced at the surface of the CE and were coupled to the SL-DOC  
690 concentration. Since the CE was relatively young (1.5 months old), autochthonous SL-DOC  
691 compounds produced by exudation ( $PP_{DOC}$ ) must have been merged with allochthonous coastal  
692 SL-DOC compounds transported during the CE formation.  $PP_{DOC}$  rates in the CE covered 28.3  
693 to 114.5% of the BCD, indicating a moderate to strong trophic dependence of bacteria on  
694 phytoplankton in CE (Fouilland and Mostajir, 2010). Although  $PP_{TOT}$  may satisfy the BCD in  
695 the CE through the bacterial incorporation of phytoplankton-derived DOC from sloppy feeding,  
696 exudation, viral infection, or cell apoptosis, a question remains about why heterotrophs  
697 preferentially used SL-DOC compounds for respiration rather than for biomass production. We  
698 start from two hypotheses, firstly, the SL-DOM compounds had a high C/N ratio leading to an  
699 increase of BR and a decrease of BGE (Lønborg et al., 2011). Secondly, SL-DOC was easier to  
700 access for bacteria than other nutrients. Phytoplankton-DOM exudate/lysates are more or less  
701 labile following their origin (e.g. diatoms/cyanobacteria) and are depleted in the nutrient (e.g.  
702 nitrate/phosphate) limiting phytoplankton growth (e.g. Pete et al., 2010; Wear et al., 2020). As  
703 the phytoplankton community was diverse within the CE and as the CE likely transported





704 allochthonous DOM, a multitude of compounds with specific qualities coexisted in the CE.  
705 Therefore, bacteria may have used SL-DOC as fuel to degrade DOM compounds containing  
706 limiting nutrients for their growth (Guillemette et al., 2016).

707 The diversity of DOM from different origins (e.g. cyanobacteria/diatom) within the CE likely  
708 induced distinct bacterial communities. We noticed a negative semilogarithmic relationship  
709 (Fig 6) between cell-specific BR and the BGE in both the zonal transect (coastal+open ocean  
710 stations) and the CE influenced (CE + Frontal Zone) stations. The slopes of the curves and the  
711 ranges of cell-specific BR values were different between the two systems suggesting distinct  
712 bacterial communities with different degrees of resource optimization (Baña et al., 2014).  
713 Within the CE, the bacterial community was probably as the phytoplankton community even  
714 more diverse as observed in previous CEs studies (Zhang et al., 2011; Yan et al., 2018).

715 Our results show that bacteria do not grow proportionally to the amount of DOM they received  
716 through exudation but rather depends on the different requirement between respiration and  
717 biomass production. In response, the BGE varied sevenfold within the CE (1.4-10.5%) whereas  
718 it varied twofold in the open ocean (0.9-2.3%) and in the coastal (5.3-7.9%) stations. Robinson  
719 (2008) suggested that most of the BGE variability within oligotrophic waters is explained by  
720 BR. Here we hypothesise that in CEs, which cross oligotrophic waters in the ETNA, BGE  
721 variability depends on both BP through phytoplankton taxonomical composition and BR  
722 through the amount and quality of the SL-DOC.

723 Overall, we showed that autotrophy prevails in the upper 100m depth of Mauritanian coastal  
724 waters while heterotrophy prevailed offshore. This is coherent with a modeling study from  
725 Lovecchio et al. (2017). The CE and the associated Frontal Zone fuelled phytoplankton  
726 nutrients needs and maintained autotrophy offshore. The highest  $PP_{TOT}$  and the most  
727 pronounced autotrophy were determined at the Frontal Zone. Mouriño-Carballido (2009)  
728 reported from indirect estimations of net community production that the frontal zones between  
729 CEs and ACEs are among the most productive area in the North West subtropical Atlantic  
730 Ocean. Previous studies showed that the trophic balance could switch from autotrophy to  
731 heterotrophy in an eddy within a month(s) (Maixandeu et al., 2003; Mouriño-Carballido et al.,  
732 2006). Here we report with a small timescale (11 days) that in a CE, states of little to high  
733 autotrophy occurred. Thus, phytoplankton dynamic and associated bacterial responses within  
734 eddies not only change with time but also through space. This urges the need for more high-  
735 resolution eddy studies in order to better estimate their impact on plankton metabolic activities  
736 and carbon cycling.



## 737 Conclusion

738

739 Our results highlight the ability of a CE to be an autotrophic vector towards the open ocean  
740 with organic matter freshly produced by the phytoplankton community inside. Yet, despite the  
741 strong autotrophy associated with the CE, phytoplankton exudation of DOM was not always  
742 enough to compensate for bacterial metabolic needs. Even if BP was enhanced in the CE, the  
743 BGE was low and varied substantially. This implies that heterotrophic bacteria recycle  
744 allochthonous DOM transported by the eddy and/or have issues to degrade phytoplankton DOM.  
745 Microbial metabolic activities dynamic within eddies are complex and require further  
746 investigations to understand and unravel the carbon cycling.

747

## 748 Data availability

749

750 All data will be made available at the PANGEA database (data manager, webmaster: Hela  
751 Mehrtens)

## 752 Author contribution

753

754 QD, KWB and AE designed the scientific study, analyzed the data and wrote the paper. AB,  
755 did the eddy reconstruction and both AE and JH commented on the paper.

756

## 757 Competing interests:

758

759 The authors declare that they have no conflict of interest.

760

## 761 Acknowledgments

762

763 We thank the captain and the crew of the *R/V Meteor* for their support during the M156 cruise.  
764 We thank J. Roa, T. Klüver and L. Scheidemann for sampling on board. We thank J. Roa and  
765 S. Golde additionally for the analysis of dissolved organic matter and T. Klüver for cell  
766 counting, bacterial and phytoplankton activities analyses. We thank B. Domeyer and R.



767 Suhrberg for the nutrient analyses. This study has been conducted using E.U. Copernicus  
768 Marine Service Information. The results contain modified Copernicus Climate Change Service  
769 information 2020. Neither the European Commission nor ECMWF is responsible for any use  
770 that may be made of the Copernicus information or data it contains. This study is a contribution  
771 of the REEBUS project (Role of Eddies in the Carbon Pump of Eastern Boundary Upwelling  
772 Systems) sub-projects WP1 and WP4, funded by the BMBF (funding reference no. 03F0815A).

773

## 774 Reference

775

776 Agustí, S., and Duarte, C. M.: Phytoplankton lysis predicts dissolved organic carbon release  
777 in marine plankton communities, *Biogeosciences*, 10, 1259-1264,  
778 <https://doi.org/10.5194/bg-10-1259-2013>, 2013.

779 Alonso-Sáez, L., Gasol, J. M., Arístegui, J., Vilas, J. C., Vaqué, D., Duarte, C. M., and  
780 Agustí, S.: Large-scale variability in surface bacterial carbon demand and growth efficiency  
781 in the subtropical northeast Atlantic Ocean, *Limnol. Oceanogr.*, 52, 533-546,  
782 <https://doi.org/10.4319/lo.2007.52.2.0533>, 2007.

783 Anderson, T. R., and Ducklow, H. W.: Microbial loop carbon cycling in ocean  
784 environments studied using a simple steady-state model, *Aquat. Microb. Ecol.*, 26, 37-49.  
785 2001.

786 Arístegui, J., Barton, E. D., Álvarez-Salgado, X. A., Santos, A. M. P., Figueiras, F. G.,  
787 Kifani, S., Hernández-León, S., Mason, E., Machú, E., and Demarcq, H.: Sub-regional  
788 ecosystem variability in the Canary Current upwelling, *Prog. Oceanogr.*, 83, 33-48,  
789 <https://doi.org/10.1016/j.pocean.2009.07.031>, 2009.

790 Arístegui, J., Montero, M. F., Hernández-Hernández, N., Alonso-González, I. J., Baltar, F.,  
791 Calleja, M. L., and Duarte, C. M.: Variability in Water-Column Respiration and Its  
792 Dependence on Organic Carbon Sources in the Canary Current Upwelling Region, *Front.*  
793 *Earth Sci.*, 8, 1-12. <https://doi.org/10.3389/feart.2020.00349/>, 2020.

794 Arístegui, J., Tett, P., Hernández-Guerra, A., Basterretxea, G., Montero, M. F., Wild, K.,  
795 Sangrá, P., Hernández-León, S., Cantón, M., García-Braun, J. A., Pacheco, M., and Barton,  
796 E. D.: The influence of island-generated eddies on Chl a distribution: a study of mesoscale  
797 variation around Gran Canaria, *Deep-Sea Res.*, 44:71-96. 1997.



- 798 Baltar, F., Arístegui, J., Gasol, J. M., Lekunberri, I., & Herndl, G. J.: Mesoscale eddies:  
799 Hotspots of prokaryotic activity and differential community structure in the ocean. *ISME*  
800 *J.*, 4, 975-988, <https://doi.org/10.1038/ismej.2010.33>, 2010.
- 801 Baña, Z., Abad, N., Uranga, A., Azúa, I., Artolozaga, I., Unanue, M., Iriberry, J., Arrieta, J.  
802 M., and Ayo, B.: Recurrent seasonal changes in bacterial growth efficiency, metabolism  
803 and community composition in coastal waters. *Environ. Microbiol.*, 22, 369-380,  
804 <https://doi.org/10.1111/1462-2920.14853>. 2020.
- 805 Baña, Z., Ayo, B., Marrasé, C., Gasol, J. M., and Iriberry, J.: Changes in bacterial  
806 metabolism as a response to dissolved organic matter modification during protozoan  
807 grazing in coastal Cantabrian and Mediterranean waters, *Environ. Microbiol.*, 16, 498-511,  
808 <https://doi.org/10.1111/1462-2920.12274>, 2014.
- 809 Bergkvist, J., Klawonn, I., Whitehouse, M. J., Lavik, G., Brüchert, V., & Ploug, H.:  
810 Turbulence simultaneously stimulates small- and large-scale CO<sub>2</sub> sequestration by chain-  
811 forming diatoms in the sea. *Nat. Commun.*, 9, 1-10, [https://doi.org/10.1038/s41467-018-](https://doi.org/10.1038/s41467-018-05149-w)  
812 [05149-w](https://doi.org/10.1038/s41467-018-05149-w), 2018.
- 813 Bergstedt, M. S., Hondzo, M. M., and Cotner, J. B.: Effects of small scale fluid motion on  
814 bacterial growth and respiration, *Freshw. Biol.*, 49, 28-40, [https://doi.org/10.1046/j.1365-](https://doi.org/10.1046/j.1365-2426.2003.01162.x)  
815 [2426.2003.01162.x](https://doi.org/10.1046/j.1365-2426.2003.01162.x), 2004.
- 816 Briand, E., Pringault, O., Jacquet, S., and Torrétón, J. P.: The use of oxygen microprobes to  
817 measure bacterial respiration for determining bacterioplankton growth efficiency. *Limnol.*  
818 *Oceanogr. Meth.*, 2, 406-416, <https://doi.org/10.4319/lom.2004.2.406>, 2004.
- 819 Busch, K., Endres, S., Iversen, M. H., Michels, J., Nöthig, E. M., and Engel, A.: Bacterial  
820 colonization and vertical distribution of marine gel particles (TEP and CSP) in the arctic  
821 Fram Strait, *Front. Mar. Sci.*, 4, 1-9. <https://doi.org/10.3389/fmars.2017.00166>, 2017.
- 822 Carr, M. E.: Estimation of potential productivity in Eastern Boundary Currents using remote  
823 sensing, *Deep-Sea Res. II: Top. Stud. Oceanogr.*, 49, 59-80, [https://doi.org/10.1016/S0967-](https://doi.org/10.1016/S0967-0645(01)00094-7)  
824 [0645\(01\)00094-7](https://doi.org/10.1016/S0967-0645(01)00094-7), 2001.
- 825 Cheney, R. E., and Richardson, P. L.: Observed Decay of a Cyclonic Gulf Stream Ring,  
826 *Deep-Sea Res. Oceanogr. Abstr.*, 23, 143-155, [https://doi.org/10.1016/S0011-](https://doi.org/10.1016/S0011-7471(76)80023-X)  
827 [7471\(76\)80023-X](https://doi.org/10.1016/S0011-7471(76)80023-X), 1976.



- 828 Couespel, D., Lévy, M., & Bopp, L.: Oceanic primary production decline halved in eddy-  
829 resolving simulations of global warming, *Biogeosciences*, 18(14), 4321-4349,  
830 <https://doi.org/10.5194/bg-18-4321-2021>, 2021.
- 831 D'Asaro, E. A.: Generation of submesoscale vortices: A new mechanism, *J. Geophys. Res.*,  
832 93, 6685-6693, <https://doi.org/10.1029/JC093iC06p06685>, 1988.
- 833 del Giorgio, P. A., and Cole, J. J.: Bacterial Growth Efficiency in Natural Aquatic Systems.  
834 *Annu. Rev. Ecol. Evol. Syst.*, 29, 503-541,  
835 <https://doi.org/10.1146/annurev.ecolsys.29.1.503>, 1998.
- 836 Demarcq, H. and Somoue, L.: Phytoplankton and primary productivity off Northwest  
837 Africa. In: *Oceanographic and biological features in the Canary Current Large Marine*  
838 *Ecosystem*. Valdés, L. and Déniz-González, I. (eds). IOC-UNESCO, Paris. IOC Technical  
839 Series, No. 115, pp. 161-174. URI: <http://hdl.handle.net/1834/9186.2015>.
- 840 Descy, J. P., Leporeq, B., Viroux, L., François, C., & Servais, P.: Phytoplankton production,  
841 exudation and bacterial reassimilation in the River Meuse (Belgium). *J. Plankton Res.*,  
842 24(3), 161-166. <https://doi.org/10.1093/plankt/24.3.161>, 2002.
- 843 Dickson, A. G., Sabine, C. L., and Christian, J. R.: *Guide to Best Practices for Ocean CO<sub>2</sub>*  
844 *measurements*. PICES Special Publication 3, 191 pp., 2007.
- 845 Dittmar, T., Cherrier, J., and Ludwichowski, K. U.: *The analysis of amino acids in seawater,*  
846 *in: Practical guidelines for the analysis of seawater*, ed. by Oliver Wurl Boca Raton [u.a.],  
847 CRC Press, ISBN: 978-1-4200-7306-5, 2009.
- 848 Dray, S.: On the number of principal components: A test of dimensionality based on  
849 measurements of similarity between matrices, *Comput. Stat. Data Anal.*, 52, 4, 2228-2237,  
850 2008.
- 851 Eichinger, M., Sempéré, R., Grégori, G., Charrière, B., Poggiale, J. C., and Lefèvre, D.:  
852 Increased bacterial growth efficiency with environmental variability: Results from DOC  
853 degradation by bacteria in pure culture experiments, *Biogeosciences.*, 7(6), 1861-1876,  
854 <https://doi.org/10.5194/bg-7-1861-2010>, 2010.
- 855 Engel, A., and Galgani, L.: The organic sea-surface microlayer in the upwelling region off  
856 the Coast of Peru and potential implications for air-sea exchange processes. *Biogeosciences*,  
857 13(4), 989-1007, <https://doi.org/10.5194/bg-13-989-2016>, 2016.



- 858 Engel, A., Goldthwait, S., Passow, U., and Alldredge, A.: Temporal decoupling of carbon  
859 and nitrogen dynamics in a mesocosm diatom bloom. *Limnol. Oceanogr.* 47, 753-761, doi:  
860 10.4319/lo.2002.47.3.0753, 2002.
- 861 Engel, A., Händel, N., Wohlers, J., Lunau, M., Grossart, H. P., Sommer, U., and Riebesell,  
862 U.: Effects of sea surface warming on the production and composition of dissolved organic  
863 matter during phytoplankton blooms: Results from a mesocosm study, *J. Plankton Res.*,  
864 33(3), 357-372, <https://doi.org/10.1093/plankt/fbq122>, 2011.
- 865 Evans, C. A., O'Reily, J. E., and Thomas, J. P.: A handbook for measurement of Chl a a  
866 and primary production, College Station, TX: Texas A &M University, 1987.
- 867 Ewart, C. S., Meyers, M. K., Wallner, E. R., McGillicuddy, D. J., and Carlson, C. A.:  
868 Microbial dynamics in cyclonic and anticyclonic mode-water eddies in the northwestern  
869 Sargasso Sea, *Deep-Sea Res. II: Top. Stud. Oceanogr.*, 55(10-13), 1334-1347.  
870 <https://doi.org/10.1016/j.dsr2.2008.02.013>, 2008.
- 871 Falkowski, P. G., Ziemann, D., Kolber, Z., and Bienfang P. K.: Role of eddy pumping in  
872 enhancing primary production in the ocean, *Letters to Nature*, Vol 352, 1991.
- 873 Feng, M., Majewski, L. J., Fandry, C. B., and Waite, A. M.: Characteristics of two counter-  
874 rotating eddies in the Leeuwin Current system off the Western Australian coast, *Deep-Sea*  
875 *Res. II: Top. Stud. Oceanogr.*, 54(8-10), 961-980,  
876 <https://doi.org/10.1016/j.dsr2.2006.11.022>, 2007.
- 877 Fischer, T., Karstensen, J., Dengler, M., and Bendinger, A.: Multiplatform observation of  
878 cyclonic eddies during the REEBUS experiment, EGU General Assembly 2021, online, 19-  
879 30 Apr 2021, EGU21-6537, <https://doi.org/10.5194/egusphere-egu21-6537>, 2021.
- 880 Gargas, E.: A Manual for Phytoplankton Primary Production Studies in the Baltic, *The*  
881 *Baltic Marine Biologists*, 2, 88 p., 1975.
- 882 Gattuso J. P., Epitalon J. M., Lavigne H. and Orr J.,: seacarb: seawater carbonate chemistry,  
883 R package version 3.2.13, <http://CRAN.R-project.org/package=seacarb>, 2020.
- 884 Gruber, N., Lachkar, Z., Frenzel, H., Marchesiello, P., Münnich, M., McWilliams, J. C.,  
885 Nagai, T., and Plattner, G. K.: Eddy-induced reduction of biological production in eastern  
886 boundary upwelling systems. *Nat. Geosci.*, 4(11), 787-792,  
887 <https://doi.org/10.1038/ngeo1273>, 2011.



- 888 Guillemette, F., Leigh McCallister, S. and del Giorgio, P.: Selective consumption and  
889 metabolic allocation of terrestrial and algal carbon determine allochthony in lake  
890 bacteria, *ISME J.*, 10, 1373-1382, <https://doi.org/10.1038/ismej.2015.215>, 2016.
- 891 Hansell, D. A., Carlson, C. A., Repeta, D. J., & Schlitzer, R.: Dissolved organic matter in  
892 the ocean a controversy stimulates new insights. *Oceanogr.*, 22(SPL.ISS. 4), 202–211.  
893 <https://doi.org/10.5670/oceanog.2009.109>, 2009.
- 894 Hernández-Hernández, N., Arístegui, J., Montero, M. F., Velasco-Senovilla, E., Baltar, F.,  
895 Marrero-Díaz, Á., Martínez-Marrero, A., and Rodríguez-Santana, Á.: Drivers of Plankton  
896 Distribution Across Mesoscale Eddies at Submesoscale Range, *Front. Mar. Sci.*, 7, 1-13.  
897 <https://doi.org/10.3389/fmars.2020.00667>, 2020.
- 898 Ihaka R., and Gentleman R.: R: a language for data analysis and graphics. *J. Comput. Graph.*  
899 *Stat.* 5, 299, 1996
- 900 Karstensen, J., Fiedler, B., Schütte, F., Brandt, P., Körtzinger, A., Fischer, G., Zantopp, R.,  
901 Hahn, J., Visbeck, M., and Wallace, D.: Open ocean dead zones in the tropical North  
902 Atlantic Ocean, *Biogeosciences*, 12, 2597-2605, <https://doi.org/10.5194/bg-12-2597-2015>,  
903 2015.
- 904 Kim, B., Kim, S. H., Kwak, J. H., Kang, C. K., Lee, S. H., & Hyun, J. H.: Heterotrophic  
905 bacterial production, respiration, and growth efficiency associated with upwelling intensity  
906 in the Ulleung Basin, East Sea. *Deep Sea Res. Part II Top. Stud. Oceanogr.*, 143, 24-35,  
907 <https://doi.org/10.1016/j.dsr2.2017.07.002>, 2017.
- 908 Kirchman, D., K'nees, E., and Hodson, R.: Leucine incorporation and its potential as a  
909 measure of protein synthesis by bacteria in natural aquatic systems, *Appl. Environ.*  
910 *Microbiol.*, 49(3), 599-607, <https://doi.org/10.1128/aem.49.3.599-607.1985>, 1985.
- 911 Lasternas, S., and Agustí, S.: The percentage of living bacterial cells related to organic  
912 carbon release from senescent oceanic phytoplankton, *Biogeosciences*, 11, 6377-6387,  
913 <https://doi.org/10.5194/bg-11-6377-2014>, 2014.
- 914 Lasternas, S., Piedeleu, M., Sangrà, P., Duarte, C. M., and Agustí, S.: Forcing of dissolved  
915 organic carbon release by phytoplankton by anticyclonic mesoscale eddies in the  
916 subtropical NE Atlantic Ocean. *Biogeosciences*, 10(3), 2129-2143,  
917 <https://doi.org/10.5194/bg-10-2129-2013>, 2013.



- 918 Lathuilière, C., Echevin, V., and Lévy, M.: Seasonal and intraseasonal surface Chl a-a  
919 variability along the northwest African Coast, *J. Geophys. Res. Oceans*, 113, C05007.  
920 <https://doi.org/10.1029/2007JC004433>, 2008.
- 921 Le Vu, B., Stegner, A., Arsouze, T.: Angular momentum eddy detection and tracking  
922 algorithm (AMEDA) and its application to coastal eddy formation, *J. Atmos. Oceanic*  
923 *Technol.* 35, 739-762. <https://doi.org/10.1175/JTECH-D-17-0010.1>, 2018.
- 924 Lee, M. M., and Williams, R. G.: The role of eddies in the isopycnic transfer of nutrients  
925 and their impact on biological production, *J. Mar. Res.*, 58(6), 895-917,  
926 <https://doi.org/10.1357/002224000763485746>, 2000.
- 927 Lévy, M., Klein, P., and Treguier, A. M.: Impact of submesoscale physics on production  
928 and subduction of phytoplankton in an oligotrophic regime, *J. Mar. Res.*, 59(4), 535-565,  
929 2001.
- 930 Lindroth P., Mopper K.: High performance liquid chromatographic determination of  
931 subpicomole amounts of amino acids by precolumn fluorescence derivatization with o-  
932 phthaldialdehyde, *Anal. Chem.*, 51, 1667-1674, <https://doi:10.1021/ac50047a019>, 1979.
- 933 Lochte, K., and Pfannkuche, O.: Cyclonic cold-core eddy in the eastern North Atlantic. II.  
934 Nutrients, phytoplankton and bacterioplankton, *Mar. Ecol. Prog. Ser.*, 39, 153-164.  
935 <https://doi.org/10.3354/meps039153>, 1987.
- 936 López-Urrutia, Á., and Morán, X. A. G.: Resource limitation of bacterial production distorts  
937 the temperature dependence of oceanic carbon cycling, *Ecology*, 88(4), 817-822,  
938 <https://doi.org/10.1890/06-1641>, 2007.
- 939 Löscher, C. R., Fischer, M. A., Neulinger, S. C., Fiedler, B., Philippi, M., Schütte, F., Singh,  
940 A., Hauss, H., Karstensen, J., Körtzinger, A., Künzel, S., and Schmitz, R. A.: Hidden  
941 biosphere in an oxygen-deficient Atlantic open-ocean eddy: Future implications of ocean  
942 deoxygenation on primary production in the eastern tropical North Atlantic,  
943 *Biogeosciences*, 12, 7467-7482, <https://doi.org/10.5194/bg-12-7467-2015>, 2015.
- 944 Lovecchio, E., Gruber, N., & Münnich, M: Mesoscale contribution to the long-range  
945 offshore transport of organic carbon from the Canary Upwelling System to the open North  
946 Atlantic. *Biogeosciences*, 15(16), 5061–5091. <https://doi.org/10.5194/bg-15-5061-2018>,  
947 2018.





- 948 Lovecchio, E., Gruber, N., Münnich, M., and Lachkar, Z.: On the long-range offshore  
949 transport of organic carbon from the Canary Upwelling System to the open North Atlantic,  
950 *Biogeosciences*, 14(13), <https://doi.org/10.5194/bg-14-3337-2017>, 2017.
- 951 Mahadevan, A.: The Impact of Submesoscale Physics on Primary Productivity of Plankton,  
952 *Annu. Rev. Mar. Sci.*, 8, 161-184, <https://doi.org/10.1146/annurev-marine-010814-015912>,  
953 2016.
- 954 Maixandeau, A., Lefevre, D., Karayanni, H., Christaki, U., VanWambeke, F., Thyssen, M.,  
955 Denis, M., Fernandez, C.I., Uitz, J., Leblanc, K., Queguiner, B.: Microbial community  
956 production, respiration, and structure of the microbial food web of an ecosystem in the  
957 northeastern Atlantic Ocean, *J. Geophys. Res. Oceans*, 110 (C7), C07S17, 2005.
- 958 Marañón E, Cermeño P, Fernández E, Rodríguez J, Zabala L.: Significance and mechanisms  
959 of photosynthetic production of dissolved organic carbon in a coastal eutrophic ecosystem,  
960 *Limnol Oceanogr*, 49, 1652–1666, 2004.
- 961 Marbá, N., Duarte, C. M., and Agustí, S.: Allometric scaling of plant mortality rate, *P. Natl.*  
962 *Acad. Sci. USA*, 104, 15777–15780, 2007.
- 963 McGillicuddy Jr, D. J., Anderson, L. A., Doney S. C., and Maltrud, M. E.: Eddy-driven  
964 sources and sinks of nutrients in the upper ocean : Results from a 0 . 1 ° resolution model  
965 of the North Atlantic, *Glob. Biogeochem. Cycles.*, 17(2), 1035,  
966 <https://doi.org/10.1029/2002GB001987>, 2003.
- 967 McGillicuddy, D. J., and Robinson, A. R.: Eddy-induced nutrient supply and new  
968 production in the Sargasso Sea, *Deep-Sea Res. I: Oceanogr. Res. Pap.*, 44(8), 1427-1450,  
969 [https://doi.org/10.1016/S0967-0637\(97\)00024-1](https://doi.org/10.1016/S0967-0637(97)00024-1), 1997.
- 970 McGillicuddy, D. J.: Mechanisms of Physical-Biological-Biogeochemical Interaction at the  
971 Oceanic Mesoscale, In *Annual Review of Marine Science* (Vol. 8),  
972 <https://doi.org/10.1146/annurev-marine-010814-015606>, 2016.
- 973 Mied, R. P., J. C. McWilliams, and Lindemann G. J.: The generation and evolution  
974 of mushroom-like vortices, *J. Phys. Oceanogr.*, 21,489-510, 1991.
- 975 Molemaker, M. J., McWilliams, J. C., and Dewar, W. K.: Submesoscale generation of  
976 mesoscale anticyclones near a separation of the California Undercurrent, *J. Phys.*  
977 *Oceanogr.*, 45, 613-629, <https://doi.org/10.1175/JPO-D-13-0225.1>, 2015.



- 978 Mouriño-Carballido, B., and McGillicuddy, D. J.: Mesoscale variability in the metabolic  
979 balance of the Sargasso Sea, *Limnol. Oceanogr.*, 51(6), 2675-2689,  
980 <https://doi.org/10.4319/lo.2006.51.6.2675>, 2006.
- 981 Mouriño-Carballido, B.: Eddy-driven pulses of respiration in the Sargasso Sea, *Deep-Sea*  
982 *Res. I: Oceanogr. Res. Pap.*, 56(8), 1242-1250, <https://doi.org/10.1016/j.dsr.2009.03.001>,  
983 2009.
- 984 Neijssel, O. M., and Mattos, M. J. T. De.: Micro Review The energetics of bacterial growth  
985 : a reassessment, 13(2), 179-182, 1994.
- 986 Nielsen, E. S.: The use of radio-active carbon (c14) for measuring organic production in the  
987 sea, *ICES Mar. Sci.*, 18(2), 117-140, <https://doi.org/10.1093/icesjms/18.2.117>, 1952.
- 988 Noyon, M., Morris, T., Walker, D., & Huggett, J.: Plankton distribution within a young  
989 cyclonic eddy off south-western Madagascar, *Deep Sea Res. Part II Top. Stud. Oceanogr.*,  
990 166, 141-150, <https://doi.org/10.1016/j.dsr2.2018.11.001>, 2018.
- 991 Passow, U.: Transparent exopolymer particles (TEP) in aquatic environments, *Prog.*  
992 *Oceanogr.*, 55(3-4), 287-333, [https://doi.org/10.1016/S0079-6611\(02\)00138-6](https://doi.org/10.1016/S0079-6611(02)00138-6), 2002.
- 993 Pete, R., Davidson, K., Hart, M. C., Gutierrez, T., and Miller, A. E. J.: Diatom derived  
994 dissolved organic matter as a driver of bacterial productivity: The role of nutrient limitation,  
995 *J. Exp. Mar. Biol. Ecol.*, 391(1-2), 20-26, <https://doi.org/10.1016/j.jembe.2010.06.002>,  
996 2010.
- 997 Rao, D. N., Chopra, M., Rajula, G. R., Durgadevi, D. S. L., and Sarma, V. V. S. S.: Release  
998 of significant fraction of primary production as dissolved organic carbon in the Bay of  
999 Bengal, *Deep Sea Res. Part I Oceanogr. Res.*, 168, 1-27,  
1000 <https://doi.org/10.1016/j.dsr.2020.103445>, 2021.
- 1001 Regaudie-De-Gioux, A., and Duarte, C. M.: Temperature dependence of planktonic  
1002 metabolism in the ocean. *Glob. Biogeochem. Cycles*, 26(1), GB1015,  
1003 <https://doi.org/10.1029/2010GB003907>, 2012.
- 1004 Reinthaler, T., Bakker, K., Manuels, R., van Ooijen, J., & Herndl, G. J.: Erratum to Fully  
1005 automated spectrophotometric approach to determine oxygen concentrations in seawater  
1006 via continuous-flow analysis. *Limnol. Oceanogr. Methods* 5(1), 72-72.  
1007 <https://doi.org/10.4319/lom.2007.5.72>, 2007.



- 1008 Robinson C.: Heterotrophic bacterial respiration. In: Kirchman DL (ed) Microbial ecology  
1009 of the oceans, Wiley-Liss, New York, NY., 2008.
- 1010 Russell, J. B. and Cook, M. G.: Energetics of Bacterial Growth : Balance of Anabolic and  
1011 Catabolic Reactions, *Microbiol Rev.*, 59(1), 48-62, 1995.
- 1012 Schartau, M., Engel, A., Schröter, J., Thoms, S., Völker, C., and Wolf-Gladrow, D.:  
1013 Modelling carbon overconsumption and the formation of extracellular particulate organic  
1014 carbon, *Biogeosciences*, 4, 433-454, 2007.
- 1015 Schlitzer, R.: Ocean Data View, [odv.awi.de](http://odv.awi.de), 2020.
- 1016 Schütte, F., Brandt, P., and Karstensen, J.: Occurrence and characteristics of mesoscale  
1017 eddies in the tropical northeastern Atlantic Ocean, *Ocean Sci.*, 12, 663-685,  
1018 <https://doi.org/10.5194/os-12-663-2016>, 2016.
- 1019 Seymour, J. R., Amin, S. A., Raina, J. B., and Stocker, R.: Zooming in on the phycosphere:  
1020 The ecological interface for phytoplankton-bacteria relationships. *Nat. Microbiol.*, 2,  
1021 17065, <https://doi.org/10.1038/nmicrobiol.2017.65>, 2017.
- 1022 Simon, M., and Azam, F.: Protein content and protein synthesis rates of planktonic marine  
1023 bacteria, *Mar. Ecol. Prog. Ser.*, 51, 201-213, 1989.
- 1024 Singh, A., Gandhi, N., Ramesh, R., & Prakash, S.: Role of cyclonic eddy in enhancing  
1025 primary and new production in the Bay of Bengal, *J. Sea Res.*, 97, 5-13,  
1026 <https://doi.org/10.1016/j.seares.2014.12.002>, 2015.
- 1027 Smith, D., and Azam, F.: A simple, economical method for measuring bacterial protein  
1028 synthesis rates in seawater using. *Mar. Microb. Food Webs*, 6(2), 107-114, 1992.
- 1029 Solorzano, L.: Determination of Ammonia in Natural Waters by the Phenolhypochlorite  
1030 Method, *Limnol. Oceanogr.*, 14, 799-801, 1969.
- 1031 Strickland, J.D.H. and Parsons, T.R.: A Practical Handbook of Seawater Analysis. Bulletin  
1032 of Fisheries Research Board of Canada, 167, 1-311, 1968.
- 1033 Thomsen, S.: The formation of a subsurface anticyclonic eddy in the Peru-Chile  
1034 Undercurrent and its impact on the near-coastal salinity, oxygen, and nutrient distributions,  
1035 *J. Geophys. Res. Oceans*, 121, 476-501, <https://doi.org/10.1002/2015JC010878>, 2016.



- 1036 Thornton, D. C. O.: Dissolved organic matter (DOM) release by phytoplankton in the  
1037 contemporary and future ocean, *Eur. J. Phycol.*, 49(1), 20-46,  
1038 <https://doi.org/10.1080/09670262.2013.875596>, 2014.
- 1039 Vaqué, D., Alonso-Sáez, L., Aristegui, J., Agustí, S., Duarte, C. M., Montserrat Sala, M.,  
1040 Vázquez-Domínguez, E., and Gasol, J. M.: Bacterial production and losses to predators  
1041 along an Open ocean productivity gradient in the Subtropical North East Atlantic Ocean. *J.*  
1042 *Plankton Res.*, 36(1), 198-213, <https://doi.org/10.1093/plankt/fbt085>, 2014.
- 1043 Wear, E. K., Carlson, C. A., and Church, M. J.: Bacterioplankton metabolism of  
1044 phytoplankton lysates across a cyclone-anticyclone eddy dipole impacts the cycling of  
1045 semi-labile organic matter in the photic zone, *Limnol. Oceanogr.*, 65(7), 1608-1622,  
1046 <https://doi.org/10.1002/lno.11409>, 2020.
- 1047 Wickham H.: tidyverse: Easily Install and Load ‘Tidyverse’ Packages. See [https://cran.r-](https://cran.r-project.org/package=tidyverse)  
1048 [project.org/package=tidyverse](https://cran.r-project.org/package=tidyverse), 2016.
- 1049 Wilhelm, W. L.: Die Bestimmung des im Wasser gelösten Sauer- stoffes, *Ber. Dtsch. Chem.*  
1050 *Ges.*, 21, 2843-2854, 1888.
- 1051 Wood, A. M., and van Valen, L. M.: Paradox lost? On the release of energy-rich compounds  
1052 by phytoplankton, *Mar. Microb. Food Webs*, 4, 103-116, 1990.
- 1053 Xu, G., Dong, C., Liu, Y., Gaube, P., and Yang, J.: Chl a Rings around Ocean Eddies in the  
1054 North Pacific, *Sci. Rep.*, 9(1), 1-8, <https://doi.org/10.1038/s41598-018-38457-8>, 2019.
- 1055 Xu, J., Jing, H., Sun, M., Harrison, P. J., and Liu, H.: Regulation of bacterial metabolic  
1056 activity by dissolved organic carbon and viruses, *J. Geophys. Res. Biogeosci.*, 118(4), 1573-  
1057 1583, <https://doi.org/10.1002/2013JG002296>, 2013.
- 1058 Yan, W., Zhang, R., and Jiao, N.: A longstanding complex tropical dipole shapes marine  
1059 microbial biogeography, *Appl. Environ. Microbiol.*, 84(18),  
1060 <https://doi.org/10.1128/AEM.00614-18>, 2018.
- 1061 Zhang, Y., Jiao, N., Sun, Z., Hu, A., & Zheng, Q.: Phylogenetic diversity of bacterial  
1062 communities in South China Sea mesoscale cyclonic eddy perturbations, *Res. Microbiol.*,  
1063 162(3), 320–329, <https://doi.org/10.1016/j.resmic.2010.12.006>, 2011.